

MASTER THESIS

# CT-BASED MIGRATION ANALYSIS OF TIBIAL COMPONENTS IN TOTAL KNEE ARTHROPLASTY

N.N. DE LAAT

Graduation internship Technical Medicine  
Leiden University Medical Centre – Department of Orthopedics

*Graduation committee:*

Chairman  
Medical Supervisor  
Technical Supervisor UT  
Technical Supervisor LUMC  
Supervisor Profession Behavior  
External Member

Prof. dr. ir. C.H. Slump  
Prof. dr. R.G.H.H. Nelissen  
Prof. dr. ir. C.H. Slump  
Dr. ir. B.L. Kaptein  
Drs. R.M. Krol  
Dr. ir. A.M. Leferink

*Date:*  
June 29<sup>th</sup> 2022

# ACKNOWLEDGEMENTS

This thesis is the final product of the research that I conducted during a 10 month internship for Technical Medicine at the department of Orthopedics in Leiden University Medical Center (LUMC).

I would like to take a moment to express my gratitude to the people who helped me during this period.

First of all, I would like to thank Bart Kaptein for supervising me and thereby answering numerous questions. Likewise, I am grateful to Rob Nelissen who provided knowledge and expertise with enthusiasm. Furthermore, I would like to thank Kees Slump for the useful insights during the (digital) update sessions, where I was stimulated too look through those 'blue eyes'. I am profoundly grateful to Ruby Krol for the contribution to my personal development, which included finding Jack Sparrow's compass. Additionally, I would like to thank Erwin Luesink for the creative digital explanation of mathematics and Esther de Rooij for proof reading my master thesis. Similarly, I would like to thank Marjelle Scheffers, Lennard Koster and Jessica Barends for their editing help. Thanks should also go to the clinicians, researchers and other employees of LUMC for having a great time together.

Finally, I would like to thank all my friends and family for being supportive and understanding, especially during the final weeks when I endured large amount of stress which were not caused by my studies. And a special thanks to Daniël for the endless support during this period, and the profound technical conversations over dinner and on the beach.

I hope you enjoy reading this thesis.

Nienke de Laat

*The Hague, June 2022*

# ABSTRACT

**Introduction:** Early implant migration is considered a predictive factor of aseptic loosening in total knee arthroplasty (TKA). Relatively large initial migration, and/or continuous migration, is indicative for an increased risk of aseptic loosening. The gold standard to measure migration is currently roentgen stereophotogrammetric analysis (RSA). However, RSA is complex in common practice due to the use of a calibration cage, trained radiology personnel and insertion of bone markers. To overcome these disadvantages, a computed tomography (CT) based method has been proposed as alternative. This CT-based migration analysis (CTBMA) measures the displacement of orthopedic implants relative to the host bone over time in CT images.

**Objective:** Comparison of migration measurement in tibial components in TKA between CTBMA and model-based RSA.

**Method:** In a prospective study, tibial component migration was measured between one year (YR1) and five years (YR5) postoperative after primary TKA with CTBMA and model-based RSA. For CTBMA, the tibia (bone) and tibial component were segmented in the CT image of YR1. The underlying voxel intensities of these volumes were matched on the CT image of YR5 using image registration. The resulting rigid transformation of both volumes were used to calculate the relative displacement of the tibial component to the tibia. This resulted in translations along and rotation around X-axis (transverse), Y-axis (longitudinal) and Z-axis (sagittal). Total translations (TT) and total rotations (TR) were calculated with root sum square. Bland-Altman plots were constructed to determine the mean difference and limits of agreement (mean  $\pm$  1.96 SD) between CTBMA and RSA.

**Results:** Seventeen patients were included for the comparison of CTBMA and RSA. The mean difference was -0.07 mm [-0.46 mm to 0.33 mm] and -0.12° [-0.88° to 0.64°] for TT and TR, respectively. The limits of agreement did not exceed  $\pm$  0.5 mm for translations. For rotations the limits of agreement were: X-axis [-0.98° to 0.94°], Y-axis [-0.89° to 0.85°] and Z-axis [-0.67° to 0.51°].

**Discussion:** We showed that CTBMA is feasible for tibial components in TKA in clinical practice and that the method agrees sufficiently with RSA. Similarly to RSA, it is important to determine the clinical precision of CTBMA, which was not done in the current study, but is advised to do in future research. Overall, CTBMA seems a promising marker-free alternative to RSA for evaluation of tibial component migration in TKA in hospitals with a similar CT scanner.

# CONTENT

Acknowledgements .....	1
Abstract.....	2
Content .....	3
Abbreviations .....	4
1. Introduction .....	5
1.1 Clinical background .....	5
1.2 Roentgen stereophotogrammetric analysis (RSA) .....	6
1.3 Clinical problem .....	7
1.4 Computed tomography based migration analysis (CTBMA) .....	7
1.5 Aim.....	7
2. Outline of thesis .....	8
3. Method.....	9
3.1 Study population and data .....	9
3.2 RSA .....	9
3.3 CTBMA .....	9
3.4 Statistical analysis .....	16
3.5 Acceptable limits of agreement and sample size .....	17
4. Results.....	18
4.1 CT data .....	19
4.2 Migration analysis .....	19
5. Discussion .....	23
5.1 Comparison between CTBMA and RSA .....	23
5.2 CTBMA and other methods of migration analysis .....	23
5.3 Clinical relevance of CTBMA.....	24
5.4 Limitations to CTBMA.....	24
5.5 Strengths and limitations of this study .....	24
5.6 Future research .....	25
6. Conclusion.....	27
References .....	28
Appendix A: Development of method.....	32
Dataset A: Cadaveric bone.....	34
Dataset B: Micromanipulator .....	41
Dataset C: Clinical data .....	46
Appendix B: Bland-Altman plots .....	51
Appendix C: Histogram plots .....	53

## **ABBREVIATIONS**

<b>CAD</b>	Computer-aided design
<b>CT</b>	Computed tomography
<b>CTBMA</b>	CT-based migration analysis
<b>CTMA</b>	CT micromotion analysis
<b>CTSA</b>	CT-based spatial analysis
<b>LROI</b>	Dutch arthroplasty register (in Dutch: Landelijke Registratie Orthopedische implantaten)
<b>LUMC</b>	Leiden University Medical Center
<b>MTPM</b>	Maximal total point of motion
<b>RSA</b>	Roentgen stereophotogrammetric analysis
<b>SD</b>	Standard deviation
<b>SEMAR</b>	Single energy metal artifact reduction
<b>TKA</b>	Total knee arthroplasty
<b>TR</b>	Total rotation
<b>TT</b>	Total translation
<b>YR1</b>	One year postoperative
<b>YR5</b>	Five years postoperative

# 1. INTRODUCTION

## 1.1 CLINICAL BACKGROUND

Total knee arthroplasty (TKA) is a common treatment for knee joints that have been affected by osteoarthritis, rheumatoid arthritis, or trauma. The orthopedic surgeon replaces the damaged joint with a prosthesis. The main indication for TKA is pain, accompanied by functional limitation in daily activities. The pain is typically worsened by activity and decreases at rest. In later disease stages, it may become continuously present. Radiographic findings may be useful in confirming the diagnosis, assessing the severity of the disease and excluding other pathologic conditions. In 2019, a total of 25,881 primary TKAs were performed in the Netherlands [1]. This number is predicted to increase to approximately 150% in 2030, due to weight gain and aging of the population [2]. Unfortunately, TKAs fail for a variety of reasons, including loosening, instability, infection and persistent pain [1]. Approximately 82% of primary TKAs last 25 years [3]. Revision surgery is expensive and often results in a less favorable outcome for the patient. The choice for revision is based on clinical symptoms and is carefully weighted for each specific patient, therefore, revision percentages differ by, but are not limited to, patient, procedure and prosthesis characteristics. In 2019, a total of 3096 revision TKAs were performed in the Netherlands [1].

One of the most reported reason for revision is aseptic loosening (i.e. gross migration) of prosthetic components [1], [4]. Aseptic loosening refers to the failure of joint prostheses without the presence of an external mechanical cause or infection [5]. Clinical expression of aseptic loosening is often only seen after ten years. However, long term loosening starts with early micromotion, small movements of the prosthesis relative to the bone, which are already measurable during the first two postoperative years [6]. Continuous migration, a shift in position of the implant over time, may result in aseptic loosening [7], [8]. Total knee prostheses migrating below 0.5 mm at six months postoperative and below 0.2 mm at six to twelve months postoperative are classified as stable [7]. In another study, the criterium for migration was 0.2 mm/two year and migration below this value was classified as stable [6]. In this study of Ryd et al. 60 (38% of total) cases of migration were identified, of which twelve received revision surgery within eight years which confirmed loosening at revision [6]. Early migration of tibial components in TKA has been associated with long-term risk of revision, see figure 1 [6], [8], [9].

In clinical practice, loosening of prostheses is assessed in radiographs by detecting radiolucent lines around the prosthesis and visual position and orientation differences of the prosthesis. Radiolucent lines indicate the presence of a fibrous layer. For objective measurement of micromotion of orthopedic implants roentgen stereophotogrammetric analysis (RSA) was developed [10]–[12]. This radiographic technique is the gold standard to assess the migration pattern of prostheses. Measuring early micromotion is useful for prediction of future aseptic loosening [6], [13]. Therefore, RSA can be used in a phased evidence-based introduction of orthopedic implants [14], [15]. Due to the high precision of RSA, new implant designs, coatings, and surgical techniques are evaluated in small clinical trials with relative short follow up [16]. This results in lower 10-year revision rates of implants in large patient populations [17].

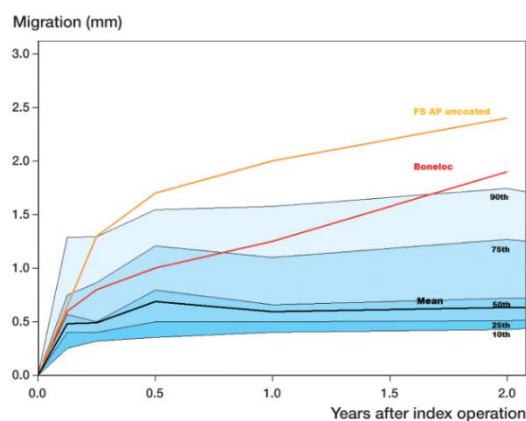


Figure 1: Early migration in percentiles of a meta-analysis of 2,470 knees. The migration of two prostheses with above average revision rates is also plotted: Boneloc cement and Freeman-Samuelson allpoly uncemented and uncemented. Image reproduced from [7].

## 1.2 ROENTGEN STEREOPHOTOGRAMMETRIC ANALYSIS (RSA)

In 1974, RSA was introduced by Goran Selvik as method for kinematics of the skeletal system [12]. Nowadays, RSA is used as the gold standard for measuring three-dimensional micromotion of joint implants relative to the bone [16], [18]. For RSA, small roentgen opaque markers of Tantalum are used as artificial landmarks, see figure 2. These markers, with a diameter of 0.5, 0.8, or 1.0 mm, are inserted into the bone during primary TKA. In conventional RSA the prosthesis is marked as well. However, implants manufactured with special markers increases costs and time. Therefore, from 2000 onwards model-based RSA is used, which renders prosthesis markers unnecessary. This technique calculates the position and orientation of a triangulated surface model by matching the virtual projection of this model to the actual projected contours of the implant. [19], [20]

A standard RSA set-up contains two roentgen tubes at an angle of  $20^\circ$  positioned approximately 1.5 m above a calibration box, see figure 2. The calibration cage is positioned underneath the table on which the patient is placed and contains a calibration grid which is used as a coordinate system to reconstruct the three-dimensional positions of the projection of the markers. The bone markers function as a reference rigid body relative to which the motion of the second rigid body, the prosthesis, is calculated. Thereafter, the relative motion of the prosthesis with respect to the bone is calculated. The results from the calculations are a rotation matrix and a translation vector. For practical interpretation, the migration is usually expressed as the difference in position and orientation of the center of the prosthesis.

Precision and accuracy of RSA differ for the axes, for specific implant designs and for different joints, which can be explained by the underlying technique. Therefore the ranges mentioned here are the standard deviation (SD) of tibial components in TKA from worst to best axis. Precision should be tested *in vivo* with double examinations, in contrast to accuracy which is tested only in *in vitro* experiments [11], [21]–[23]. Clinical precision of model-based RSA for tibial components at one year postoperative varies from 0.03 mm to 0.21 mm (SD) for translations and from  $0.08^\circ$  to  $0.61^\circ$  (SD) for rotations [24]. The accuracy of model-based RSA is calculated by the difference between measured and applied motion, in this case with the use of a 3D computer-aided design (CAD) model of the tibia; the standard deviation varies from 0.10 mm to 0.21 mm (SD) and  $0.39^\circ$  to  $0.81^\circ$  (SD) for translation and rotation measurements respectively [25].

Accuracy of a measurement can be described as “the degree of closeness between a measured value and the true value and contains both random and systemic errors”. The precision of a measurement is described as “the degree to which repeated measurements under unchanged condition show the same results”. [26]

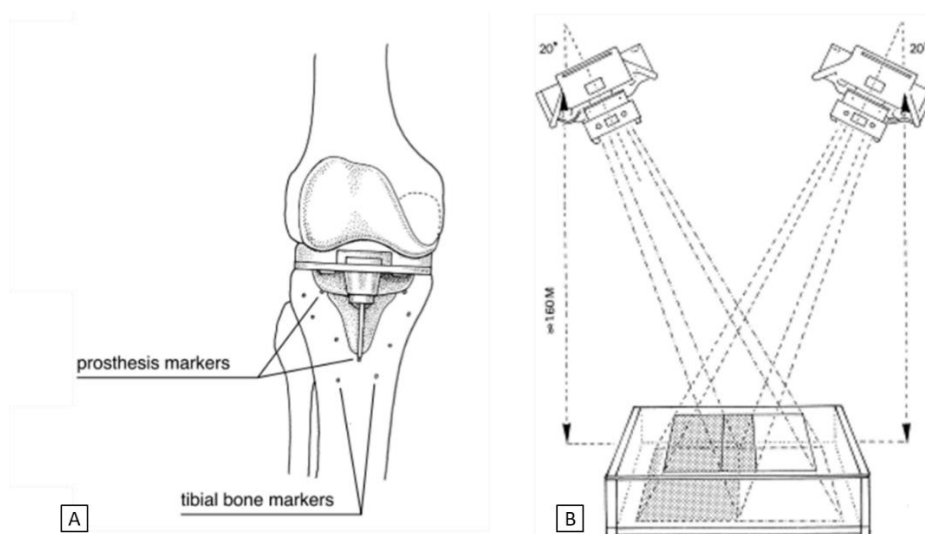


Figure 2: A) Total knee prosthesis with seven Tantalum markers inserted in the tibia, and three markers attached to the prosthesis. Image reproduced from [10]. B) The RSA set-up consists of two separate roentgen tubes with corresponding digital radiography detector and one calibration cage. The imaging body part is positioned on top of the calibration cage at the joint of interest of the X-ray bundles. Two separate roentgen images are taken virtually simultaneously. Image was used with permission [27].

### 1.3 CLINICAL PROBLEM

Although RSA is the current gold standard to measure implant migration, it has some disadvantages. RSA requires the insertion of bone markers, making the technique unsuitable for evaluation of implant loosening in patients who were not given such markers initially. Also, the required instrument to insert tantalum markers, as well as the markers themselves, are not yet approved by the updated medical device regulation for use in clinical studies. RSA is sensitive for marker occlusion due to over-projection by the implant. Moreover, an expensive set-up and trained personnel are needed to conduct and analyze examinations. Recently, the use of computed tomography (CT) scans was introduced as an alternative method for measurement of prosthesis migration [28]–[30]. This CT-based method for migration analysis provides more hospitals the opportunity to test orthopedic implants, since CT scanners are widely available. For the use in clinical research, the accuracy and precision of this method should be in the same order as RSA and the advantages should outweigh the disadvantages.

### 1.4 COMPUTED TOMOGRAPHY BASED MIGRATION ANALYSIS (CTBMA)

There is no universal terminology used for the CT-based method in the literature. We propose the following term: CT-based migration analysis (CTBMA). CTBMA is a method which measures migration of orthopedic implants over time in CT images. *In vitro* [31], [32] and *in vivo* [33]–[35] studies indicate that the accuracy and precision of CTBMA are comparable to those of RSA. In the literature, several methods for CTBMA are used with different terminology. Two studies validated a commercially available software called CT micromotion analysis (CTMA) in acetabular cups of patients [34], [35]. CTMA uses surface registration for the spatial alignment of the images. Scheerlinck et al. were the first to describe CTBMA without the use of markers or manually placed landmarks: CT-based spatial analysis (CTSA) [31]. In *in vitro* experiments the limits of agreement between imposed motion and measurement were within  $\pm 0.28$  mm for translations and  $\pm 0.20^\circ$  for rotations in any direction [31]. They obtained segmentation masks of the prosthesis and the bone, and used the voxel intensities of the original image for the registration. This spatial alignment of the images was used to calculate the displacement of the prosthesis relative to the bone between baseline and follow-up, see figure 3. In contrast to CTMA, CTSA uses volume registration.

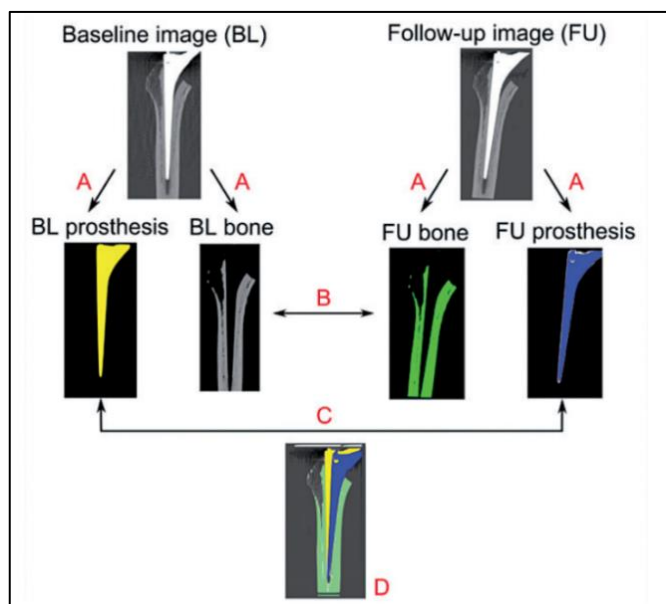


Figure 3: Visual example of the CT-based spatial analysis method of hip implants. A represents segmentation, B and C represents the registration of the volumes of bone and prosthesis respectively. D visualizes the migration of the prosthesis relative to the bone. The yellow, green and blue area represents the volume masks of the prosthesis, bone, and prosthesis, respectively. Image reproduced from [31].

### 1.5 AIM

The aim of this study is to investigate CTBMA, based on the method of Scheerlinck et al., in TKA. Furthermore, we aim to develop a clinical usable segmentation algorithm for defining masks. Leiden University Medical Center (LUMC) uses Mimics (Materialise) for segmentation in 3D planning of orthopedic surgeries. The advantage of this segmentation software is the intuitive use and the in house expertise since it is also used for 3D planning of operations. For these reasons, we want to define the masks by segmentation in Mimics. The accuracy of Mimics has been investigated in the literature [36], [37]. Firstly, a segmentation algorithm will be developed in Mimics for clinical CT images of knees after TKA. Secondly, this segmentation algorithm is used for CTBMA and this method is compared to the gold standard of migration measurement. The aim is formulated in the following research question: **What is the difference between CTBMA and model-based RSA in migration measurements of tibial components in TKA?**



## 2. OUTLINE OF THESIS

In order to answer the research question, first, multiple experiments were conducted to develop an usable method of CTBMA. These experiments, described in **appendix A**, focused on a clinical usable segmentation algorithm together with improvement of image registration. These experiments contributed to the method of CTBMA as described in **chapter 3** of this master thesis. The results of comparison between CTBMA and RSA for seventeen patients were described in **chapter 4**. Hereafter, **chapter 5** includes an extensive discussion on strengths and limitations whilst also focusing on future research. Finally, **chapter 6** includes an overall conclusion of this master thesis.

## 3. METHOD

The primary output of this study was the migration of the tibial component relative to the tibia bone. This migration was measured with two different methods: RSA and CTBMA.

### 3.1 STUDY POPULATION AND DATA

Data was obtained from a prospective randomized clinical trial previously conducted at the Orthopaedic department of LUMC comparing the migration of two types of tibial designs with RSA: the Persona PS and the NexGen LPS [24]. Inclusion criteria were patients aged between 21 and 90 years scheduled for primary TKA, between 2014 and 2017, for osteoarthritis or rheumatoid arthritis [24]. In an addendum to the study, with a separate informed consent, one extra postoperative CT scan was added. Follow-up involved a CT scan and a pair of radiographs for RSA at one and five years postoperatively. All imaging was performed on the same day. Only patients who received a CT scan at one year follow-up were invited for the CT scan at five year follow-up.

The randomized controlled trial included 75 patients. All patient data was anonymized for the researcher. The data collection of these patients at five year follow-up is ongoing. Therefore, we used a data cutoff point at the 7<sup>th</sup> of January 2022. Data analysis was carried out with all data available until this date. Patients were excluded for follow-up when: (1) markers in baseline RSA were insufficient for both bones, (2) CT scan at one year follow-up was missing, (3) the implant had been revised, and (4) patient was unable or unwilling to sign the additional informed consent. Patients were excluded from data analysis if CT follow-up was incomplete and if the slice thickness of CT images was more than 0.5 mm. For this study the two types of tibial designs are combined to one group, since the aim is to compare CTBMA to the gold standard and not to compare the two tibial designs.

### 3.2 RSA

RSA radiographs were acquired using two X-ray sources angled at 40 degrees towards each other in combination with digital radiography detectors and a calibration cage. Details were described previously [24]. RSA was performed using model-based RSA software (v. 4.2014, RSAcore; LUMC, The Netherlands). Data analysis with RSA was conducted only in patients who were included for data analysis of CTBMA. The migration was calculated between one and five years postoperative images, in contrast to the RSA study where migration was calculated with direct postoperative as starting point [24].

### 3.3 CTBMA

CTBMA is a method that measures displacement of orthopedic implants relative to the host bone over time in CT images. In general, CTBMA consists of four steps; (1) data acquisition, (2) mask defining, (3) registration, and (4) calculation of migration, see figure 4. The development of method was in consultation with experiments as described in appendix A.

For data acquisition, CT scans were obtained of one year (YR1) and five years (YR5) after TKA. These images were analyzed with a novel in-house graphical user interface called CTRSA-software (Python v3.9.7, CTRSA-software, date: 02-04-2022) to measure migration between two rigid bodies, more specifically, the tibial component and the tibia (bone). In order to do this, three masks were obtained by segmentation: an align mask, a mask of the bone, and a mask of the prosthesis. These masks were used for the initial alignment of the image, the bone-bone registration and prosthesis-prosthesis registration, respectively. The intensities of the underlying voxels of these masks were used for image registration. This intensity-based image registration with mask volumes was performed using Elastix, a toolbox for medical image registration [38]. The migration was then calculated from the transformations. The four steps of CTBMA are described in detail below.

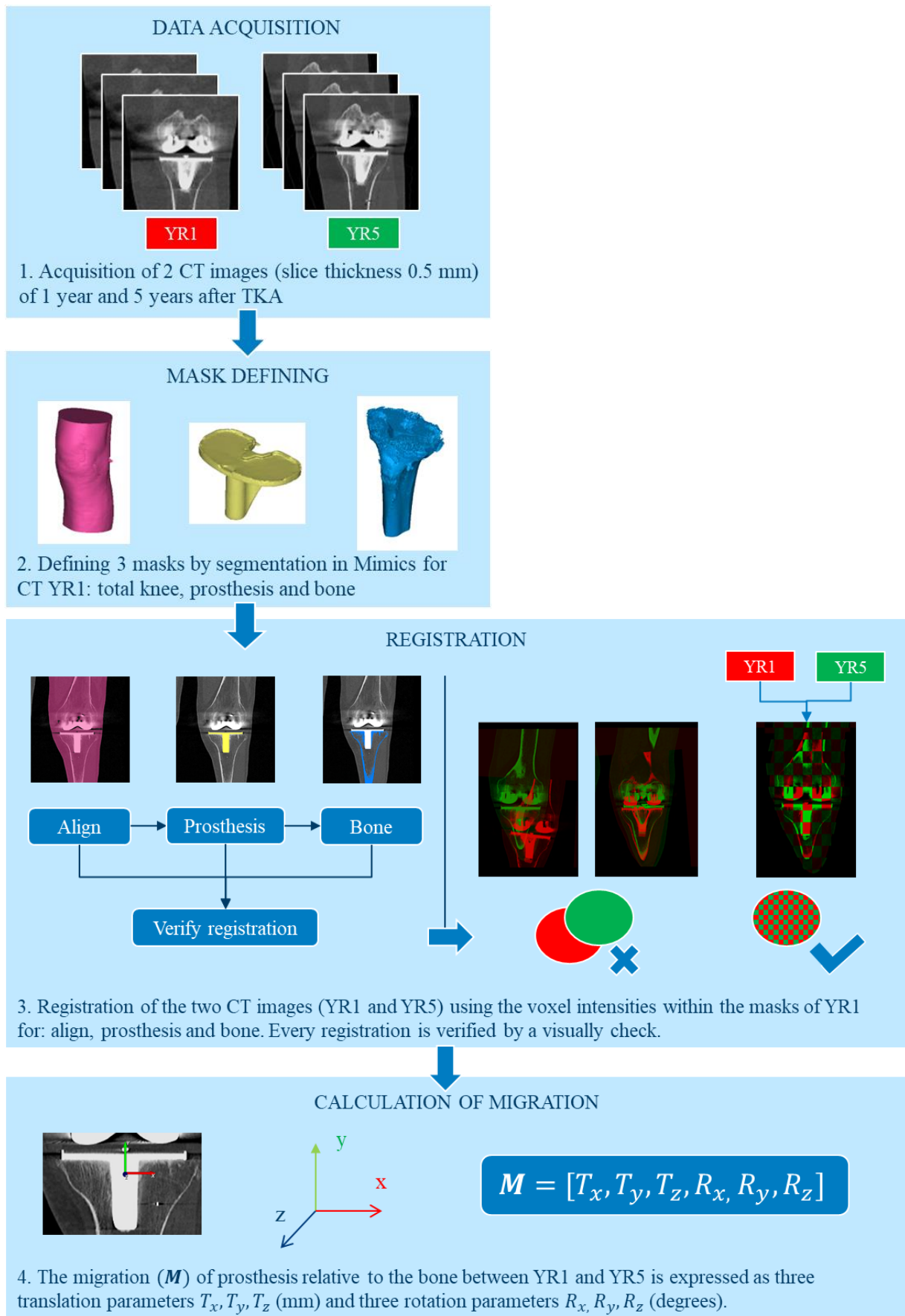


Figure 4: Schematic overview of the four steps of CTBMA to calculate the migration of the prosthesis relative to the bone between YR1 and YR5. Image registration was performed by means of a graphical user interface, which allows visual verification of the registration.

### 3.3.1 Data acquisition

CT images with a slice thickness of 0.5 mm were acquired with two different CT scanners (Canon, Aquilion and Aquilion ONE). These CT scans were conducted during normal working hours at the radiology department. All images were reconstructed with both a bone filter (convolution kernel FC30) and some images with the single energy metal artifact reduction (SEMAR) reconstruction technique. For every CT image the following parameters were documented: CT scanner, helical or volume, CT tube voltage (kVp), data collection diameter, CT tube current (mA), reconstruction diameter, convolution kernel, focal spot (mm), pixel spacing (mm) and dose (mGy). The matrix size was 512x512, the beam collimation 80 x 0.5 mm for helical scans and max 16 cm for volume scans, and the rotation was 0.5 (sec) for both helical and volume. The pixel spacing equals the pixel size assuming the space between pixels is zero and is equal in both directions. Note that in this report the pixel size is referred to as the smallest addressable element of the image, given in millimeters. This is one of the contributing factors for the spatial resolution of the image.

### 3.3.2 Mask defining

Three masks were obtained by segmentation; (1) mask of the total knee for the initial alignment, (2) mask of tibia bone, and (3) mask of tibial component of prosthesis. The CT images of YR1 of all patients were used for the segmentation. The whole segmentation process was carried out in a commercial software package (Mimics, Materialise, Belgium). The first step of the segmentation in all masks was thresholding. This threshold was derived from a line intensity profile with a tradeoff between segmented object and surroundings, and was chosen for each CT image separately, see figure 5. To extract the prosthesis, a threshold was applied to the image followed by a region grow of 6-connectivity. The seed was placed inside the tibial component in TKA. Next, a morphological operation of erode followed by a dilate (open) and a dilate followed by an erode (close) of 1 pixel was applied to the mask. This was useful for breaking small connections and for filling cavities within the mask. To extract the tibia bone, another threshold was applied to include the bone pixels, but exclude the tantalum bone markers (RSA markers). This threshold was followed by a region grow. Next, an orthogonal cut was made between prosthesis and bone to exclude the metal artifacts caused by the prosthesis, see figure 5c. A Boolean operation was then performed to exclude the prosthesis from the bone (negation, subtraction). For the align mask, another threshold was applied to include soft tissue of the knee. When needed, in case of two knees or a table, the crop function was used to select the required knee. All three segmentation objects were applied to the CT image of YR1, thereby retaining the voxel intensities within the segmented objects.

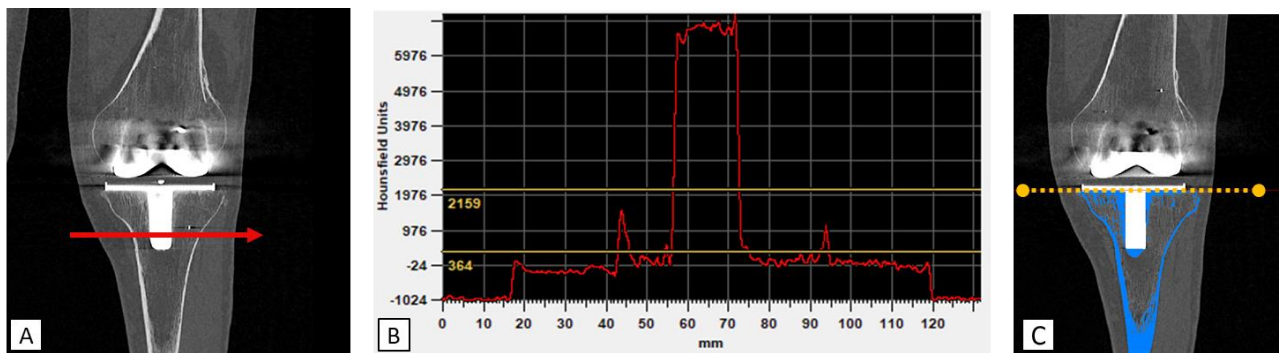


Figure 5: A) Draw profile line (red arrow) through soft tissue, bone and prosthesis for a line intensity profile. The arrow is enlarged for illustration purposes. B) Defining the threshold (horizontal orange lines) for the bone mask, which is a tradeoff between soft tissue and bone, using the line intensity profile (red line). C) Orthogonal cut (dashed orange line) was made where tibial plateau and tibia meets.

### 3.3.3 Registration

Registration is the spatial alignment of two or more images. In the current study, registration was performed with CT images of one year (YR1) and five years (YR5) postoperatively using only the voxel intensities within the defined masks instead of the whole image. The volume registration was performed using Elastix; a toolbox for intensity-based medical image registration [38]. Image registration was described as “the task of finding a spatial transformation mapping from one image to another” [39].

The three-dimensional gray-scale image  $I$  in spatial domain  $\Omega$  assigns to every point  $x \in \Omega \subset \mathbb{R}^3$  a normalized gray value  $I(x) \in [0,1]$  (called the intensity value at the point  $x$  of that image). Two images are needed for the registration: the *moving image*  $I_M = I(x) \forall x \in \Omega_M \subset \mathbb{R}^3$  and the *fixed image*  $I_F = I(x) \forall x \in \Omega_F \subset \mathbb{R}^3$ . The mapping from one image to the other results in a coordinate transformation  $A(x)$  that makes  $I_M(x)$  spatially aligned with  $I_F(x)$  [38]. In Elastix, for practical reasons, this transformation  $A$  was defined as a mapping from the fixed image to the moving image. The alignment optimization was estimated by minimizing the cost function, see equation (1). [39]

$$\hat{A} = \arg \min_A C(A; I_F, I_M) \quad (1)$$

In Elastix specific parameters can be chosen to optimize the quality of the alignment. The following parameters were used: multiresolution registration, linear interpolator, normalized correlation metric, and an adaptive stochastic gradient descent optimizer.

Three registrations were performed using the voxel intensities within the three defined masks and therefore a labeled subset  $L$  of points  $x \in L_F \in \Omega_F$ . All three registration methods used a multiresolution strategy:

1. Align registration: This first registration was a rough alignment of the two images using the voxel intensities within the align mask. More specifically, the registration was performed with fewer number of iterations in each resolution level of the multiresolution approach. Also, in this registration the moving image can only be translated and not rotated.
2. Prosthesis-prosthesis registration: This second registration used the align registration as starting point. The voxel intensities within the prosthesis mask were used for the registration of images. The moving image can be translated and rotated.
3. Bone-bone registration: This third registration used the registration of the prosthesis as starting point. The voxel intensities within the bone mask were used for the registration of images. The moving image can be translated and rotated.

All three registrations were visually checked in the graphical user interface (CTRSA-software) for each patient. To verify the registration the two images were displayed on top of each other with a checkerboard view and in red/green, as seen in figure 4. The researcher then assessed continuous borders of prosthesis and bone and considered the registration successful if the specific registration part of the two images (YR1 and YR5) do overlap completely.

### 3.3.4 Calculation of migration

The migration of the tibial component relative to the tibia bone between baseline and follow-up image, was calculated by determining the relative movement of the two volumes (i.e. tibial component and tibia) with respect to a fixed migration coordinate system. The tibial component and tibia bone were assumed as rigid bodies, hence the transformations consisted of combinations of rotations and translations only. These transformations were expressed in homogenous coordinates to combine the translations and rotations in one matrix. The movement of a rigid body in three-dimensional space consisted of 6 degrees of freedom: 3 translations along the X-axis, Y-axis, and Z-axis and 3 rotations around these axes. These rotations were determined by the right hand rule and expressed in Euler angles, whilst the angles do not exceed  $360^\circ$ .

The following equations were used to calculate the migration:

In equation (2) the rigid transformation was defined as a transformation that, when acting on any vector  $v$ , where  $v = [x, y, z, 1]^T$ , and produces a transformed vector  $v'$ :

$$v' = Av \quad (2)$$

$A$  described in homogeneous coordinates gives a 4x4 matrix  $A^{[4,4]}$ :

$$A^{[4,4]} = \begin{bmatrix} [R^{[3,3]}] & [T^{[3,1]}] \\ 0 & 0 & 0 & 1 \end{bmatrix} = \begin{bmatrix} r_{11} & r_{12} & r_{13} & p \\ r_{21} & r_{22} & r_{23} & q \\ r_{31} & r_{32} & r_{33} & r \\ 0 & 0 & 0 & 1 \end{bmatrix} \quad (3)$$

In this transformation matrix  $A$  of equation (3),  $R^{[3,3]}$  and  $r_{11}$  to  $r_{33}$  represents the rotation matrix, and  $T^{[3,1]}$  and  $p, q, r$  represents the translation vector. The mathematical representation of the transformation of a point  $(x, y, z)$  towards another point  $(x', y', z')$  in a three-dimensional space is seen in equation (4):

$$\begin{bmatrix} x' \\ y' \\ z' \\ 1 \end{bmatrix} = \begin{bmatrix} r_{11} & r_{12} & r_{13} & p \\ r_{21} & r_{22} & r_{23} & q \\ r_{31} & r_{32} & r_{33} & r \\ 0 & 0 & 0 & 1 \end{bmatrix} \cdot \begin{bmatrix} x \\ y \\ z \\ 1 \end{bmatrix} \quad (4)$$

By definition, the estimated transformation matrix  $\hat{A}$  as calculated by Elastix is defined as a mapping from the fixed image  $I_F$  to the moving image  $I_M$ , so that:

$$I_M \sim \hat{A} I_F \quad (5)$$

Where  $\hat{A}$  is the estimated transformation resulting from alignment optimization. The transformation with a subset of pixels of the fixed image  $L_F$  for the alignment is given by:

$$L_F' = \hat{A} L_F \quad (6)$$

Where  $L_F'$  is the transformed of  $L_F$  which Elastix tries to align to  $L_M$  so that:

$$L_F' \sim L_M \quad (7)$$

The reverse transformation yields:

$$L_M' = \hat{A}^{-1} L_M \quad (8)$$

Where  $L_M$  represents a specific subset of the moving image which Elastix tries to align to  $L_F$  of the fixed image (labeled by segmentation) to make  $L_M'$  (the transformed of  $L_M$ ) aligned with  $L_F$  so that:

$$L_M' \sim L_F \quad (9)$$

See figure 6.

Note that the reverse transformation is only true if the determinant of  $A$  does not equal zero.

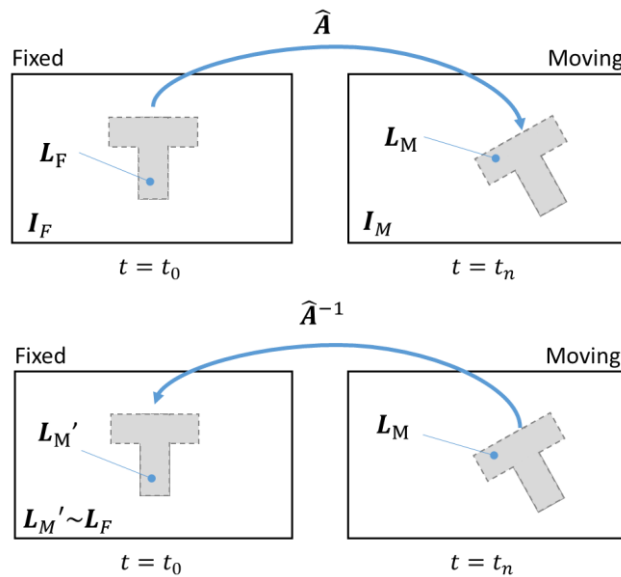


Figure 6: The estimated transformation  $\hat{A}$  is defined as the mapping from the fixed image  $I_F$  to the moving image  $I_M$  and its reverse  $\hat{A}^{-1}$  from the moving to the fixed image. The fixed image is also called the baseline ( $t = t_0$ ) and the moving image is also called the follow-up ( $t = t_n$ ). A specific subset of the fixed image  $L_F$  (labeled by segmentation) is used for the alignment optimization to a subset of the moving image  $L_M$ . Elastix optimizes alignment so that  $L_M'$  (the transformed of  $L_M$ ) is approximately equal to  $L_F$ .

In our study, Elastix optimized alignment of the bone in the moving image  $B_5$  and the bone in the fixed image  $B_1$  so that:

$$B_5' \sim B_1 \quad (10)$$

Where  $B_5'$  is the location where the bone ended up in the fixed image. In which the transformation yields:

$$B_5' = \hat{A}_B^{-1} B_5 \quad (11)$$

See figure 7.

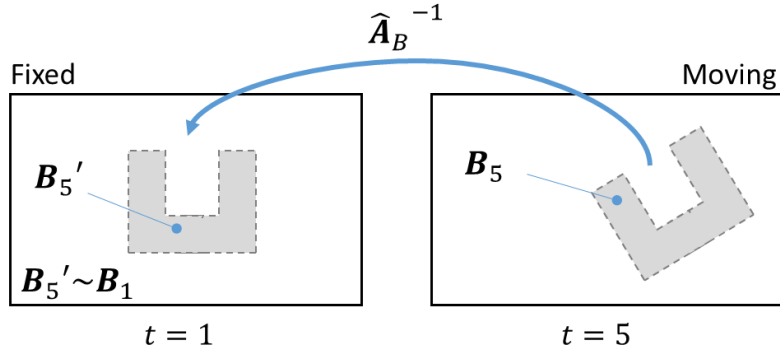


Figure 7: A graphical representation of the estimated reverse transformation of bone  $\hat{A}_B^{-1}$  from the moving to the fixed image.

Similarly, Elastix optimized alignment of the prosthesis in the moving image  $P_5$  and prosthesis in the fixed image  $P_1$  so that:

$$P_5' \sim P_1 \quad (12)$$

Where  $P_5'$  is the location where the prosthesis ended up in the fixed image. Then the transformation is given by:

$$P_5' = \hat{A}_P^{-1} P_5 \quad (13)$$

See Figure 8.

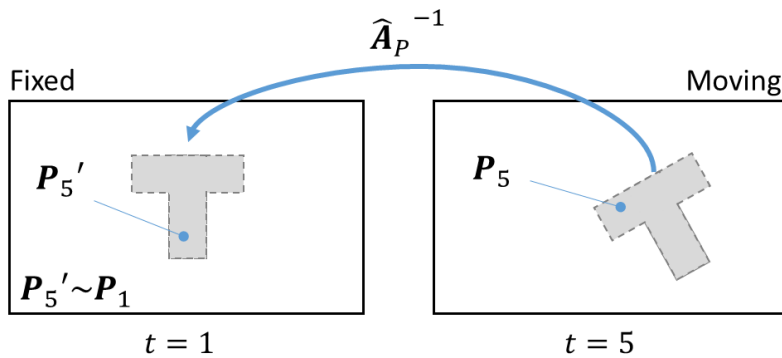


Figure 8: A graphical representation of the estimated reverse transformation of prosthesis  $\hat{A}_P^{-1}$  from the moving to the fixed image.

The relative migration over time of prosthesis with respect to the bone is of interest. Therefore, the image  $P_5$  (prosthesis in the moving image) is transformed with the bone transformation  $\hat{A}_B^{-1}$  as described in equation 14.

$$P_5'' = \hat{A}_B^{-1} P_5 \quad (14)$$

Where  $P_5''$  is the transformed of  $P_5$  whilst using the reverse transformation of bone. Migration is then characterized by the residual alignment between this image  $P_5''$  and the initial transformed image  $P_5'$  (which approaches  $P_1$ , by optimization). The migration transformation  $\hat{A}_M$  is given by:

$$P_5'' = \hat{A}_M P_5' \quad (15)$$

See Figure 9.

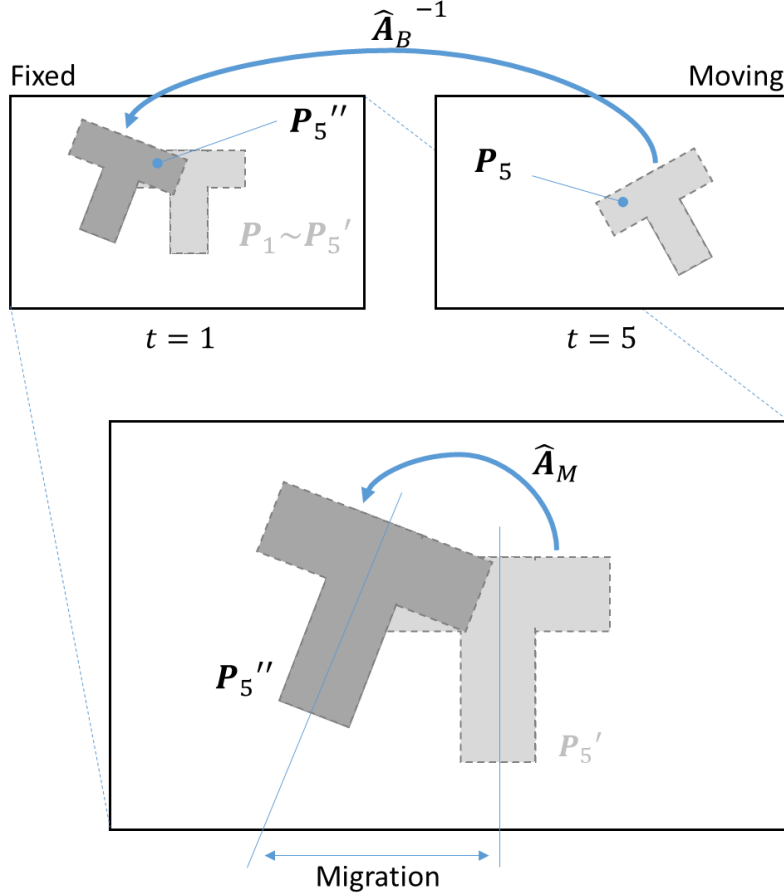


Figure 9: Migration is the relative displacement of prosthesis to the bone, between  $t = 1$  and  $t = 5$ .

By substitution, the migration transformation  $\hat{A}_M$  can hence be calculated:

$$\begin{aligned} P_5'' &= \hat{A}_M P_5' \\ \hat{A}_B^{-1} P_5 &= \hat{A}_M \hat{A}_P^{-1} P_5 \\ \hat{A}_B^{-1} &= \hat{A}_M \hat{A}_P^{-1} \\ \hat{A}_M &= \hat{A}_B^{-1} \hat{A}_P \end{aligned} \quad (16)$$

This transformation  $\hat{A}_M$  is then transformed from the global to the migrating coordinate system by:

$$\hat{A}_{M0} = A_0^{-1} \hat{A}_M A_0 \quad (17)$$

Where  $A_0$  is composed of a rotation of  $90^\circ$  around the X-axis and a translation to the center of the tibial component. This geometrical center is the calculated center of mass for a continuous mass distribution. The global coordinate system is provided by the CT image.

The migration  $M$  is then derived from function  $f$  accepting matrix  $\hat{A}_{M0}^{[4 \times 4]}$  and returning  $M^{[6 \times 1]}$ :

$$M = f(\hat{A}_{M0}) \quad (18)$$



This function  $f$  is implemented in CTRSA-software (*CTRSA\_Migration\_Calculation.py*, date: 14-04-2022, function: *matrix\_to\_parameters()*) and based on euler angle formulas [40]. The function finds the Euler angles from the rotation matrix and converts these from radians to degrees.

In equation (19),  $\mathbf{M}$  represents the migration, consisting of translations  $T_x, T_y, T_z$  in millimeters (mm) and rotations  $R_x, R_y, R_z$  in degrees (deg).

$$\mathbf{M} = [T_x, T_y, T_z, R_x, R_y, R_z] \quad (19)$$

Concluding, the displacement of the prosthesis relative to the bone, between YR1 and YR5, is given from the migrating coordinate system with its origin in the geometric center of the prosthesis. The orientation of this coordinate system equals that of RSA and is equivalent for left and right knee, see figure 6.

In general using RSA, in case of a left knee, postprocessing of the data exist of multiplying the factor -1 to  $T_x, R_y$  and  $R_z$  due to chirality, making the positive  $T_x$  direction medially and positive  $R_y$  and  $R_z$  rotation internally. This has not been done in this study because the aim was to compare the two methods.

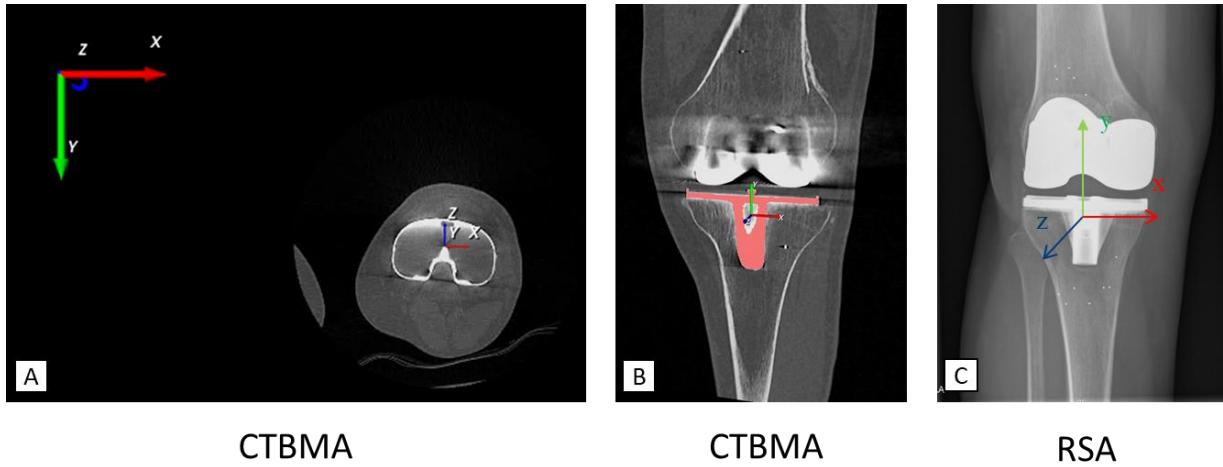


Figure 6: A) The two coordinate systems of CTBMA: the global coordinate system (left upper corner) and the migrating coordinate system with its origin in the geometric center of the tibial component (right lower corner). B) The orientation of the migrating coordinate system of CTBMA (image of left knee). C) The orientation of RSA (image of right knee). The orientation is equal for CTBMA and RSA; X-axis (transverse axis), the Y-axis (longitudinal axis) and Z-axis (sagittal axis). Rotations around these axes are according to the right hand rule.

### 3.4 STATISTICAL ANALYSIS

The total translation (TT) and the total rotation (TR) over time are calculated using root mean square, see equation (20) and (21) [12], [19]. The calculation of total rotation is only valid for small angles when  $\theta \approx 0$  and  $\sin \theta \approx \theta$ , known as small angle approximation [12].

$$TT = \sqrt{T_x^2 + T_y^2 + T_z^2} \quad (20)$$

$$TR = \sqrt{R_x^2 + R_y^2 + R_z^2} \quad (21)$$

The TT, TR, translations and rotations are compared between the two methods in a Bland-Altman plot [41]. The Bland-Altman analysis aims to compare a new measurement method against a reference standard and quantifies agreement between the two methods through the bias and limits of agreement [42]. These limits of agreements are calculated by the mean  $\pm 1.96 \times SD$ , and are then compared with a priori defined acceptable limits of agreement. The Bland-Altman analysis is visualized graphically by plotting the average of the two methods  $((CTBMA + RSA) / 2)$  on the X-axis against the difference  $(CTBMA - RSA)$  on the Y-axis (Python v3.9.7, statsmodels package v0.12.2). The plot provides the

mean difference between the two methods and the limits of agreement (mean  $\pm$  1.96 x SD) and 95% of the data will be between these limits if the data is distributed normally.

The normal distribution was visually assessed by a histogram of the difference (CTBMA – RSA) as proposed in [43]. Supplementary to the graphical assessment a Shapiro-Wilk test was conducted (Python v3.9.7, scipy package v1.7.1). The test rejects the hypothesis of normality when the p-value is less than or equal to 0.05.

A post hoc subanalysis was conducted of all patients with only one knee in the baseline and follow-up CT image. The aim of this analysis was to see if the spatial resolution of the CT images affect the agreement between CTBMA and RSA. The pixel sizes of images with two knees are larger, due to the larger field of view. Changes in the field of view will affect pixel size, considering a static matrix size of 512x512 pixels.

### 3.5 ACCEPTABLE LIMITS OF AGREEMENT AND SAMPLE SIZE

The sample size was calculated based on the limits of agreement between the two methods. These limits of agreement (mean  $\pm$  1.96xSD) should not exceed  $\pm$  0.5 mm for translation and  $\pm$  0.8° for rotations [44]. These acceptable limits of agreement were determined by [44] and were based on the smallest values of clinically relevant early migration when used as a predictor of aseptic loosening [7], [45], [46]. The pre-defined acceptable limits were conservative for TT and TR, since these limits describes a one dimensional value (and not a linear sum or root-sum-square of three values).

The calculated sample size, using the data from table 1, resulted in the minimum required number of 10 pairs for translation and 67 pairs for rotation. The expected standard deviation of differences used in this calculation was based on the data of a study comparing two techniques of RSA. The difference between CTBMA and RSA was expected to be of the same order.

Table 1: Parameters used for the calculation of sample size for translations and rotations

Type I error (alpha, significance)	0.05	
Type II error (Beta, 1-Power)	0.10	
Expected Mean of Differences	0.0	
	Translations	Rotations
Expected Standard Deviation of Differences*	0.105 mm	0.291 degrees
Maximum allowed difference	0.5 mm	0.8 degrees
Calculated minimum number of pairs	10	67

\*Data of analysis between Model-based RSA and Marker-based RSA [44]

## 4. RESULTS

Twenty patients completed CT follow-up, of which seventeen were included to compare CTBMA with RSA for migration analysis of tibial components in TKA, see flow diagram in figure 7. One patient, who did complete CT follow-up, was excluded because of incomplete RSA follow-up due to logistic reasons. In two patients, PNS30 and PNS54, the slice thicknesses of CT YR1 were larger than 0.5 mm and therefore these patients were excluded for the data analysis.

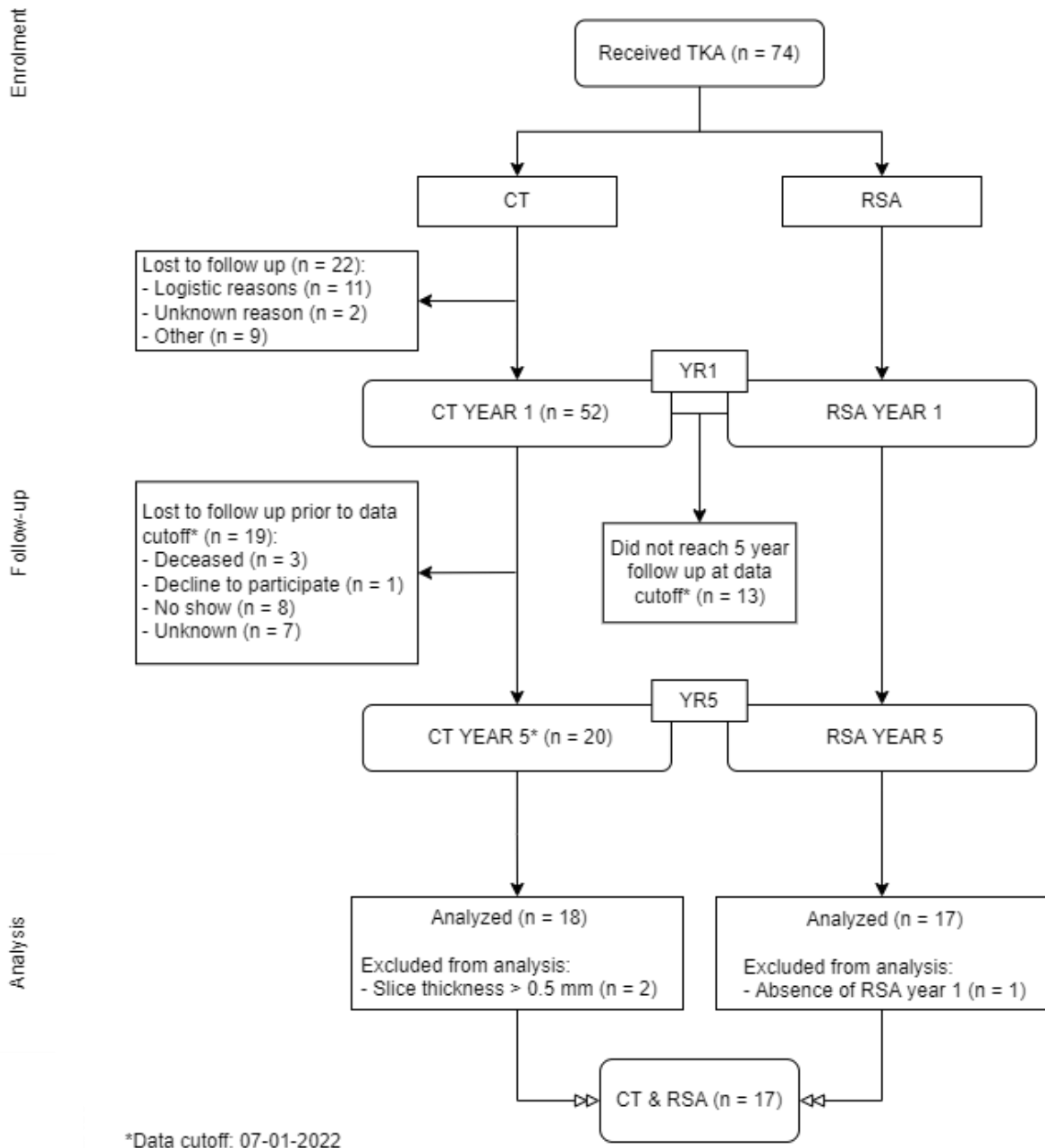


Figure 7: Flow diagram of included patients for analysis. Abbreviations: TKA = total knee arthroplasty, CT = Computed Tomography, RSA = roentgen stereophotogrammetric analysis, YR1 = one year after TKA, YR5 = five years after TKA. \*Data cutoff = 07-01-2022.

## 4.1 CT DATA

The pixel size of CT images ranged between 0.27 mm and 0.78 mm. These and other differences in CT parameters between CT images are seen in table 2.

Table 2: Overview of CT parameters. There are two CT images of each patient: one year (YR1) and five years (YR5) after primary total knee arthroplasty. All images have a slice thickness of 0.5 mm, matrix size 512x512 and convolution kernel FC30. Five images included two knees in the field of view instead of one (marked in blue). Abbreviations: # = number of patient, PNS = patient number in study, FU = follow-up, CT = Computed Tomography, kVp = kilo volt, mA = milli ampere, mm = millimeter, mGy = milli gray.

#	FU	PNS	CT scanner	Helical / volume	CT tube voltage (kVp)	Data collection diameter	CT tube current (mA)	Reconstruction diameter	Focal spot sizes (mm)	pixel spacing (mm)*	Dose (mGy)
1	YR1	12	Aquilion	HELICAL_CT	120	400	80	400	0.9\0.8	0.78	7.6
	YR5	12	Aquilion ONE	VOLUME_CT	120	500	100	210.937	0.9\0.8	0.41	2.4
2	YR1	14	Aquilion	HELICAL_CT	135	400	150	400	0.9\0.8	0.78	17.9
	YR5	14	Aquilion ONE	HELICAL_CT	120	500	110	181.64	0.9\0.8	0.35	3.8
3	YR1	15	Aquilion	HELICAL_CT	135	320	100	140	0.9\0.8	0.27	9.5
	YR5	15	Aquilion ONE	VOLUME_CT	120	400	150	321.875	0.9\0.8	0.63	7.9
4	YR1	17	Aquilion	HELICAL_CT	135	500	100	225	1.6\1.4	0.50	14.9
	YR5	17	Aquilion ONE	HELICAL_CT	120	320	100	225	0.9\0.8	0.44	6
5	YR1	19	Aquilion	HELICAL_CT	135	400	150	209	0.9\0.8	0.41	17.9
	YR5	19	Aquilion ONE	HELICAL_CT	120	500	110	218.75	0.9\0.8	0.43	3.8
6	YR1	20	Aquilion ONE	VOLUME_CT	120	400	250	217	0.9\0.8	0.42	13.2
	YR5	20	Aquilion ONE	HELICAL_CT	120	320	110	245	0.9\0.8	0.48	3.8
7	YR1	21	Aquilion ONE	HELICAL_CT	135	400	80	225	0.9\0.8	0.44	8.1
	YR5	21	Aquilion ONE	HELICAL_CT	120	320	110	203.75	0.9\0.8	0.40	4.1
8	YR1	22	Aquilion ONE	HELICAL_CT	135	320	80	190	0.9\0.8	0.37	7.2
	YR5	22	Aquilion ONE	HELICAL_CT	120	400	100	184.375	0.9\0.8	0.36	6.6
9	YR1	23	Aquilion ONE	HELICAL_CT	135	400	150	323	0.9\0.8	0.63	15.1
	YR5	23	Aquilion ONE	HELICAL_CT	120	320	110	181.25	0.9\0.8	0.35	4.1
10	YR1	25	Aquilion	HELICAL_CT	135	400	100	202	0.9\0.8	0.39	23.9
	YR5	25	Aquilion ONE	HELICAL_CT	120	320	110	257.50	0.9\0.8	0.50	4.1
11	YR1	27	Aquilion ONE	HELICAL_CT	120	400	80	344	0.9\0.8	0.67	5.8
	YR5	27	Aquilion ONE	HELICAL_CT	120	320	110	207.50	0.9\0.8	0.41	4.1
12	YR1	28	Aquilion	HELICAL_CT	135	400	80	228	0.9\0.8	0.45	19.1
	YR5	28	Aquilion ONE	HELICAL_CT	120	500	80	224.609	0.9\0.8	0.44	2.5
13	YR1	29	Aquilion ONE	VOLUME_CT	120	500	100	178	0.9\0.8	0.35	3.9
	YR5	29	Aquilion ONE	VOLUME_CT	120	400	90	182.812	0.9\0.8	0.36	4.6
14	YR1	45	Aquilion ONE	HELICAL_CT	120	500	110	191	0.9\0.8	0.37	7.2
	YR5	45	Aquilion ONE	VOLUME_CT	120	320	110	170.00	0.9\0.8	0.33	4.1
15	YR1	48	Aquilion ONE	HELICAL_CT	120	500	300	238	0.9\0.8	0.47	10.2
	YR5	48	Aquilion ONE	HELICAL_CT	135	500	110	191.406	0.9\0.8	0.37	5.3
16	YR1	50	Aquilion ONE	HELICAL_CT	120	500	200	264	1.6\1.4	0.52	16
	YR5	50	Aquilion ONE	HELICAL_CT	120	320	110	236.25	0.9\0.8	0.46	4.1
17	YR1	51	Aquilion ONE	VOLUME_CT	135	320	80	176	0.9\0.8	0.34	7.6
	YR5	51	Aquilion ONE	HELICAL_CT	120	320	110	193.75	0.9\0.8	0.38	4.1
18	YR1	58	Aquilion ONE	HELICAL_CT	135	400	80	233	0.9\0.8	0.45	8.1
	YR5	58	Aquilion ONE	HELICAL_CT	120	320	80	265	0.9\0.8	0.52	2.8

\*Pixel spacing is equal in both directions (square) and equals pixel size assuming the space between pixels is zero

## 4.2 MIGRATION ANALYSIS

Migration was measured in seventeen patients with both methods, see table 3. The prosthesis-prosthesis registration initially failed in two patients (PNS 14 and PNS 28), resulting in an visually incorrect alignment of the images. The prosthesis registration was repeated using the previous registration as starting point until verification of registration was correct. This failed registration is most likely due to the differences of rotation of the legs between the two images, because the align match only consist of a translation and does not include the option of image rotation. However, in two other patients with an imperfect align match, this did not result in an incorrect bone-bone or prosthesis-prosthesis registration. In one patient (PNS 48) RSA was not possible due to the absence of roentgen images at one year postoperatively. In another patient (PNS 15) the RSA results had to been corrected with a factor -1 for  $T_x$ ,  $T_y$ ,  $R_x$  and  $R_y$  because the roentgen images at one year postoperatively were taken upside down.

Table 3: Migration results of 18 patients measured with two methods: CTBMA and RSA. Results consists of translations (mm) along and rotations (degrees) around X-axis (transverse), Y-axis (longitudinal) and Z-axis (sagittal). All results are rounded to 2 decimals. CTBMA initially failed in PNS14 and PNS28 (marked in yellow). Abbreviations: CTBMA = CT base Migration Analysis, RSA = roentgen stereophotogrammetric analysis, TT = Total Translation, TR = Total Rotation and SD = standard deviation.

Patient	CTBMA									RSA							
	Translation (mm)			Rotation (degrees)			TT	TR	Translation (mm)			Rotation (degrees)			TT	TR	
	Tx	Ty	Tz	Rx	Ry	Rz			Tx	Ty	Tz	Rx	Ry	Rz			
1	PNS12	0.07	-0.02	-0.03	-0.20	-0.04	-0.13	0.08	0.24	0.00	0.11	0.00	-0.78	-0.35	-0.12	0.11	0.86
2	PNS14	0.03	-0.05	-0.04	-0.06	0.10	0.02	0.07	0.12	-0.02	0.04	0.13	0.11	0.60	-0.04	0.14	0.61
3	PNS15	0.16	-0.48	-0.21	-1.39	0.12	-0.84	0.55	1.63	-0.23	-0.22	-0.22	-1.35	0.32	0.09	0.39	1.39
4	PNS17	0.04	0.00	0.00	-0.20	0.18	-0.12	0.04	0.30	-0.01	0.05	0.20	-0.01	0.16	-0.01	0.21	0.16
5	PNS19	0.03	-0.21	0.01	-0.08	0.07	0.15	0.21	0.19	0.01	-0.14	0.36	0.22	0.97	-0.08	0.39	1.00
6	PNS20	-0.02	0.12	-0.09	-0.39	0.20	-0.09	0.16	0.45	-0.13	0.01	0.07	-0.13	0.06	0.13	0.15	0.19
7	PNS21	0.01	0.00	0.10	-0.26	0.04	-0.11	0.10	0.28	0.09	-0.10	0.10	-0.24	0.12	-0.07	0.17	0.28
8	PNS22	0.00	0.12	0.01	-0.09	-0.03	-0.03	0.12	0.10	-0.34	0.23	0.05	-0.66	-0.21	0.44	0.41	0.82
9	PNS23	-0.06	0.23	0.04	0.14	-0.49	-0.09	0.24	0.51	-0.03	0.13	-0.47	-0.73	0.25	-0.12	0.49	0.78
10	PNS25	0.09	-0.15	0.00	-0.62	0.67	-1.02	0.17	1.37	0.18	-0.56	0.46	0.79	-0.13	-0.80	0.75	1.13
11	PNS27	-0.06	0.17	0.03	0.08	-0.22	0.40	0.18	0.46	0.07	-0.10	0.25	-0.16	-0.08	0.16	0.28	0.24
12	PNS28	0.15	0.15	-0.06	0.05	0.30	-0.56	0.22	0.64	0.06	0.01	-0.02	-0.10	0.71	-0.07	0.06	0.72
13	PNS29	-0.12	-0.37	-0.27	-0.45	-0.05	0.30	0.48	0.54	-0.02	0.09	0.02	-0.18	-0.25	0.00	0.10	0.31
14	PNS45	-0.02	0.18	0.00	-0.75	0.24	-0.26	0.19	0.82	-0.08	-0.11	0.20	-0.79	0.40	-0.35	0.24	0.95
15	PNS48	-0.01	0.00	-0.05	-0.18	-0.03	0.03	0.05	0.19								
16	PNS50	-0.02	-0.07	-0.01	-0.03	-0.27	-0.22	0.08	0.35	0.04	0.02	0.10	-0.35	-0.94	-0.29	0.11	1.04
17	PNS51	0.00	-0.02	0.04	0.67	0.33	0.35	0.05	0.82	0.08	-0.10	0.06	0.62	-0.14	0.28	0.14	0.69
18	PNS58	0.01	0.09	-0.06	-0.43	-0.18	-0.01	0.11	0.46	-0.04	-0.02	0.06	0.01	-0.16	-0.04	0.07	0.16
Mean		0.02	-0.02	-0.03	-0.23	0.05	-0.12	0.17	0.53	-0.02	-0.04	0.08	-0.22	0.08	-0.05	0.25	0.67
SD		0.07	0.18	0.09	0.42	0.25	0.36	0.14	0.40	0.12	0.17	0.20	0.52	0.44	0.26	0.18	0.37

The mean difference for the total translation between CTBMA and RSA is -0.07 mm [mean  $\pm$  1.96 SD: -0.46, 0.33], see figure 8. The mean difference for the total rotation is -0.12° [mean  $\pm$  1.96 SD: -0.88, 0.64]. The difference of TT is normally distributed ( $p = 0.47$ ), in contrast to the difference of TR ( $p = 0.01$ ) which shows a large peak between 0.2° and 0.3°, see figure 9. In case of non-normally distributed data the limits of agreement are less informative, but as seen in the Bland-Altman plot all differences of TR are within these limits of agreement.

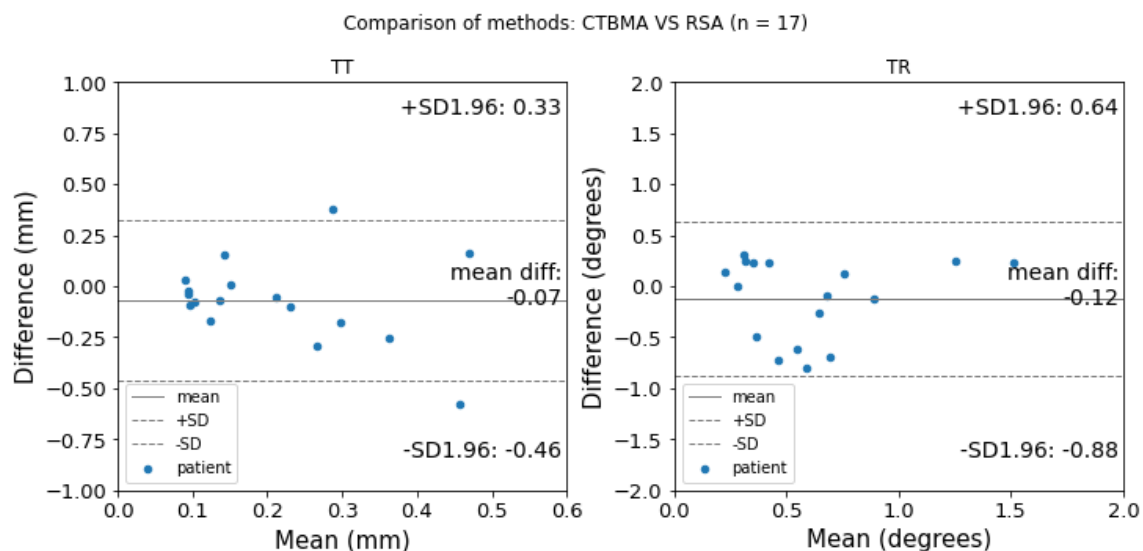


Figure 8: Bland-Altman plots of total translations (left panel) and total rotations (right panel) of seventeen patients (blue dots) for comparison between the two methods: CTBMA and RSA. The solid line is the mean difference between the two methods. The dashed lines represent the limits of agreement. Abbreviations: TT = Total Translation, TR = Total Rotation, SD = Standard Deviation, mean diff = mean difference between the two methods.

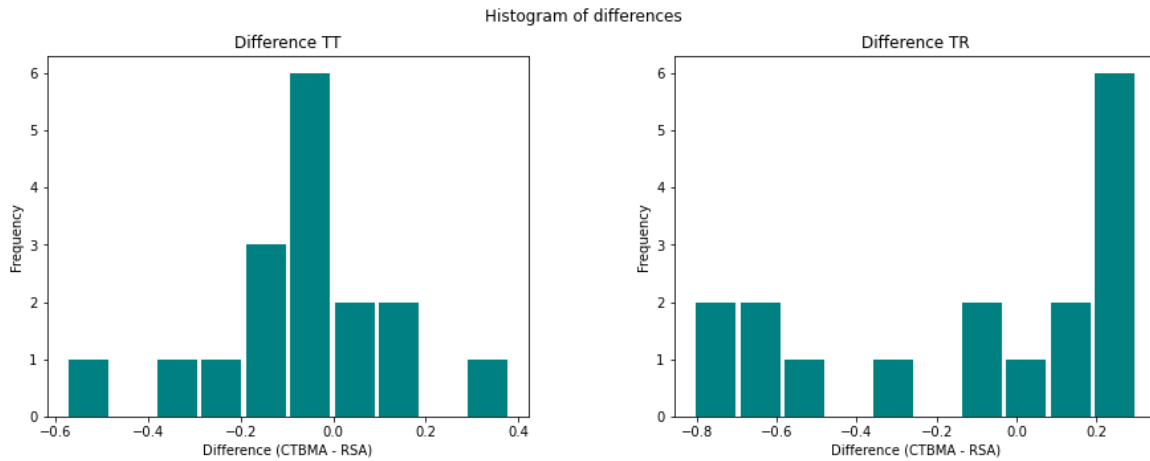


Figure 9: Histogram of differences (CTBMA – RSA) for total translations (TT) in mm and total rotations (TR) in degrees.

Twelve patients were included in the subanalysis to test if the spatial resolution of CT images affect the agreement between CTBMA and RSA. In five (28% of total) CT images two knees were imaged, corresponding with the five greatest pixel sizes (PNS12 YR1, PNS14 YR1, PNS15 YR2, PNS23 YR1, and PNS27 YR1). Without these patients, the mean difference of the TT and TR was  $-0.07$  mm [mean  $\pm$  1.96 SD:  $-0.51$ ,  $0.36$ ] and  $-0.09^\circ$  [mean  $\pm$  1.96 SD:  $-0.87$ ,  $0.68$ ], respectively, see figure 10.

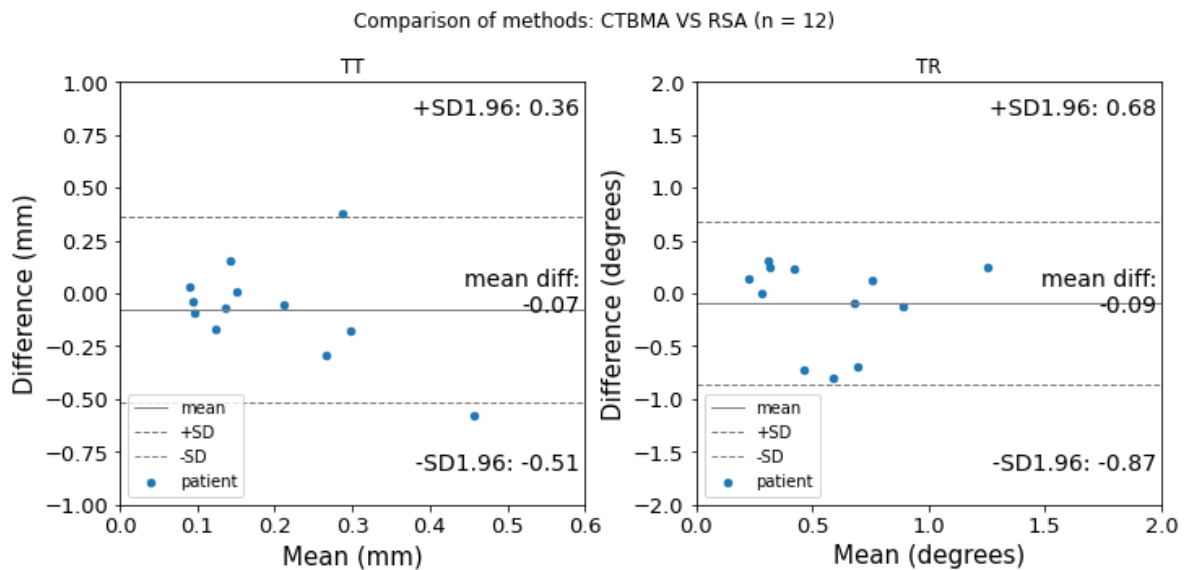


Figure 10: Bland-Altman plots of total translations (left panel) and total rotations (right panel) of 12 patients (blue dots) for comparison between the two methods: CTBMA and RSA. The solid line is the mean difference between the two methods. The dashed lines represent the limits of agreement. Abbreviations: TT = Total Translation, TR = Total Rotation, SD = Standard Deviation, mean diff = mean difference between the two methods.

Furthermore, the limits of agreement for translations and rotations between the two methods are given in table 4 for all patients, and table 5 for the subanalysis of twelve patients. The corresponding Bland-Altman plots are enclosed in appendix B and histograms in appendix C. In the subanalysis, all limits of agreement were slightly smaller, except for  $T_y$  which is the longitudinal axis and constricted to the slice thickness. The interval improved 0.25 mm and 0.25 degrees for  $T_z$  and  $R_z$  respectively. Moreover, the normal distribution of data changed between the two analysis.

Table 4: Differences of translations and rotations between CTBMA and RSA (n = 17)

Axis	Translations (mm)			Rotations (degrees)		
	Tx (transverse)	Ty (longitudinal)	Tz (sagittal)	Rx (transverse)	Ry (longitudinal)	Rz (sagittal)
Mean difference	0.04	0.02	-0.11	-0.02	-0.02	-0.08
Limits of agreement*	-0.23 to 0.31	-0.39 to 0.43	-0.5 to 0.28	-0.98 to 0.94	-0.89 to 0.85	-0.67 to 0.51
Shapiro-Wilk^	p = 0.01	p = 0.78	p = 0.02	p = 0.14	p = 0.99	p = 0.02

\*The values represent the limits of agreement between the two methods (CTBMA and RSA) and are based on all patients (n = 17)

^The test rejects the hypothesis of normality when the p-value is less than or equal to 0.05

Table 5: Subanalysis: Differences of translations and rotations between CTBMA and RSA (n = 12)

Axis	Translations (mm)			Rotations (degrees)		
	Tx (transverse)	Ty (longitudinal)	Tz (sagittal)	Rx (transverse)	Ry (longitudinal)	Rz (sagittal)
Mean difference	0.03	0.04	-0.17	-0.15	0.08	-0.06
Limits of agreement*	-0.21 to 0.26	-0.38 to 0.46	-0.43 to 0.10	-1.07 to 0.77	-0.79 to 0.94	-0.53 to 0.40
Shapiro-Wilk^	p = 0.04	p = 0.48	p = 0.33	p = 0.08	p = 0.88	p = 0.53

\*The values represent the limits of agreement between the two methods (CTBMA and RSA) and are based on patients with only one knee in CT images (n = 12)

^The test rejects the hypothesis of normality when the p-value is less than or equal to 0.05

## 5. DISCUSSION

### 5.1 COMPARISON BETWEEN CTBMA AND RSA

We compared marker-free CTBMA to RSA for evaluation of migration of the tibial component in TKA relative to the tibia (bone). Agreement between CTBMA and RSA was within pre-defined limits for TT, TR, translations in all directions, and rotations around the Z-axis, although not for rotations around the X-axis and Y-axis. The limits of agreement, [-0.46 mm to 0.33 mm] for TT and [-0.88° to 0.64°] for TR, were within the pre-defined values of  $\pm 0.5$  mm and  $\pm 0.8^\circ$  respectively.

In the current study, we assessed the agreement between the two methods and, consequently, did not provide a superior method. We compared CTBMA with RSA, the gold standard in clinical practice, in which measurement error remains possible. Therefore, we chose to compare CTBMA to RSA using a mean difference plot, described by Bland and Altman [42], assuming that the average value of two methods is closer to the truth. Superiority of methods could be tested in an experimental study where accuracy is compared to the ground truth of motion imposed by a micromanipulator.

For translations, the limits of agreement for all directions were within  $\pm 0.5$  mm. For rotations the limits of agreement should be within  $\pm 0.8^\circ$ . This limit was met for  $R_z$ , although not for  $R_x$  and  $R_y$ , which can be explained by the relative higher precision of RSA for the Z-axis compared to rotations around X-axis and Y-axis [24]. In addition, differences in  $R_y$  could partly be explained by knee rotation in the CT scanner, since the rotation of the migrating coordinate system is dependent on the orientation of the leg in the CT scanner. Likewise, the migrating coordinate system of RSA is dependent on knee alignment above the calibration box, and radiology personnel is instructed to align the knee with RSA images, but not with CT images. It is yet to be determined how alignment differences influence the results. The mismatch in alignment could be solved in CTBMA by rotating the axis in software procedures or by physically aligning the knee in the CT scanner. Furthermore, differences in measurements between CTBMA and RSA could be due to small differences in the origin of the migration coordinate system. The origin for migration is defined at the geometric center of the prosthesis, which differ for the two methods. In model-based RSA the geometric center of the prosthesis model is calculated according to a CAD model of the prosthesis. In CTBMA the origin is the geometric center of the prosthesis mask obtained by segmentation and could differ from the original prosthesis resulting in different geometric centers. Therefore, migration results could differ since these centers determine the origin of the coordinate system.

Robustness of CTBMA depends on how the different parameters in subsequent steps of the method affect the migration measurements. One of these parameters is the spatial resolution of CT images. CTBMA is expected to be limited by the voxel size of the CT images, however, our data suggest that in this dataset with varying pixel sizes the spatial resolution of the CT images is still good enough for the method to be comparable to RSA. We tested this with a subanalysis of CT images with estimated better spatial resolution. In this subanalysis of patients with only one knee in the field of view the limits of agreement did not improve for TT and TR. Also, the limits of agreement did not improve for  $R_y$  as it is constricted to the slice thickness. The limits of agreement did improve slightly for the Z-axis in the images with better spatial resolution. This improvement of 0.25 mm and 0.25° for  $T_z$  and  $R_z$  was small and may be not clinically relevant, however it does show a trend of improvement for measurement in images with better spatial resolution.

CTBMA is performed in a graphical user interface which enables optimization of registration until the registration is correct. Therefore, the user is in control of correct registration and as a consequence responsible for correct migration results. This is comparable to RSA where the user also repeats pose estimation measurements when results differ from expectations, usually when high migration values are measured.

### 5.2 CTBMA AND OTHER METHODS OF MIGRATION ANALYSIS

To the best of our knowledge, this is the first study to measure tibial component migration with CTBMA in patients and compare these results to RSA. Our method was based on Scheerlinck et al. using volume registration for alignment of rigid bodies [31]. Scheerlinck et al. evaluated *in vitro* accuracy and precision of CTBMA in hip implants. The limits of agreement for accuracy did not exceed 0.28 mm for



translations and  $0.20^\circ$  for rotations [31]. The limits of agreement for precision did not exceed 0.09 mm and  $0.14^\circ$ . This study also estimated the clinical precision of CTBMA in five patients and reported that this value was dependent on spatial resolution of CT image [31]. Another study also measured tibial component migration using volume matching, however this was MRI-based and *in vitro* [47]. The reported precision of zero motion was between 0.58 mm and 1.97 mm for translation and  $0.88^\circ$  and  $3.77^\circ$  for rotation, which was not as precise as RSA, but still showed that displacement calculation is possible using other imaging modalities. Alternatively, surface matching was used instead of volume matching [35], [48]. The reported precision for hip implants without the use of bone markers was 0.10-0.16 mm in translation and  $0.21^\circ$ - $0.31^\circ$  in rotation. Another study, in acetabular cups, compared CTBMA with RSA and determined the limits of agreement in the same way as the precision of the double RSA examination [33]. The largest limits of agreement (mean  $\pm$  1.96 SD) reported were in the sagittal axis for translations ( $T_z$ ) [-0.47 to 0.39 mm] and in the longitudinal axis for rotations ( $R_y$ ) [-1.31 to 1.21 $^\circ$ ]. Their CTBMA used tantalum beads for defining of the mask, in contrast to our marker-free method. Obviously only a marker-free method overcomes the limitations of marker use. Overall, CTBMA seems a promising marker-free alternative to RSA for migration analysis.

### 5.3 CLINICAL RELEVANCE OF CTBMA

Data collection for CTBMA could fit in normal clinical practice, resulting in a more accessible way to test new implant designs in patients. One of the main advantages of CTBMA is that this method does not require markers for migration measurement. This, in contrast to RSA, in which several markers are needed to measure migration. Hence, RSA is sensitive to marker migration and marker occlusion. Yet more importantly, CT scanners are widely available in contrast to RSA research set-ups, allowing for a more feasible evaluation of new implants using CTBMA. This adds potential to aid in resolving the quest of new implants, which guarantees quality and safety to patient care [15], [49]. Furthermore, for CTBMA no trained radiology personnel or additional equipment such as a calibration cage is needed. Still, similar to RSA, personnel is needed for data analysis. In our study, part of the analysis was conducted using a paid segmentation toolkit, but there are open-source alternatives for segmentation.

### 5.4 LIMITATIONS TO CTBMA

First, the main limitation of CTBMA compared to RSA is the higher radiation dose. The current study focused solely on the knee and especially for other joints the radiation dose might be a consideration for the applicability of CTBMA. The overall risk of radiation exposure is dependent on the specific dose absorbed by each organ and weighted for radiation type, which is quantified by the effective dose (mSv) [50]. The reported effective dose in literature is for CT scan of the knee 0.16 mSv and is for knee RSA 0.003 mSv [51], [52]. The cumulative radiation dose of CT scans in our study ranged between 2.05 and 23.90 mGy and decreased from one to five years postoperative. This decrease in radiation dose is partly explained by dose optimization, and partly by the fact that a whole leg CT was included in the one year follow-up visit, contributing to a larger cumulative dose at that time-point. Therefore, the radiation dose of CT scans in future studies should be less than our reported radiation dose.

Second, whether CTBMA robustness is compromised by material properties of prostheses is unknown. These material properties could, for example, affect metal artifacts in CT images which could challenge the use of CTBMA. In the current study, the metal artifacts surrounding the tibial component did not cause much inconvenience. However, the metal artifacts surrounding the femoral component were more present, potentially limiting the usability of CTBMA.

Third, CTBMA assumes rigid body displacement and therefore does not take possible changes in the shape or density of the bone into account. For example, osteophytes, bone remodeling, stress shielding and osteoporosis could change the aspect of the bone in follow-up imaging. This might interfere with the registration, although we did not encounter problems regarding the bone-bone registration in the current study.

### 5.5 STRENGTHS AND LIMITATIONS OF THIS STUDY

This study was the first to measure migration with CTBMA for tibial components in patients having received TKA. We have developed a novel graphical user interface for practical and easy use of image

registration and migration measurement. However, some limitations have to be considered when interpreting the results.

First, the sample size is less than the calculated required sample size (e.g. power analysis) for validation of rotation measurements. The calculated sample size was 10 TKAs for the translation and 67 TKAs for the rotation measurements. We only included seventeen patients for the analysis, hence we could only evaluate 17 TKAs.

Second, the applicability of CTBMA on migration greater than 0.55 mm and 1.63° is unknown, since we only observed migration measurements lower than these values. This is partly explained by the fact that we could only use data between one and five years postoperatively. From earlier studies we know that the majority of early migration occurs in the first six months postoperatively and then is followed by a stabilization period [7]. We could not measure the migration that occurred during the first postoperative year. Hence, we do not know the limits of agreement of CTBMA and RSA for larger migration measurements.

Third, only 20 out of 74 patients completed all CT scans during follow-up. Loss to follow-up mainly occurred between one and five years postoperatively. Chiefly, the five year follow-up period was between August 2020 and July 2022, a time during which the COVID-19 pandemic played a large role in society. Hence, this might explain the loss to follow-up during this period.

Fourth, the segmentation for defining the mask was executed by one person by hand. Although manual segmentation is often used as the ground truth [36], the method is labor intensive and prone to intra- and inter-observer variability. In our study, the threshold was set manually for each CT image independently. Also, the researcher was not an expert in segmentation. The segmentation could be standardized by automated thresholding. Alternatively, another option would have been the use of advanced segmentation methods, such as statistical shape models, which are reported to have a higher accuracy compared to manual segmentation [36]. These advanced CT image segmentation methods, however, require large training datasets which were not available. Yet another option for mask defining in general would be model-based CTBMA, similar to model-based RSA, in which the model of the prosthesis is used to identify the underlying voxels. The drawback of model-based analysis is the dependence of availability of the models. Hence, manual segmentation is currently the best available method that is usable in clinical practice.

Fifth, alignment optimization in CTBMA is sensitive to local minima resulting in incorrect registration. To overcome this problem, we used an align match for initial alignment of the images. These align masks included the bone markers of the tibia, so these may have helped the align match. Based on this initial align match, the bone and prosthesis were matched and migration was calculated. The bone markers could therefore have had an indirect effect on the results. However, in additional experiments the align match seems also possible using the prosthesis mask. Therefore, CTBMA seems to be feasible without markers.

Finally, our radiology department altered the standard knee protocol during the follow-up of this study, resulting in differences in CT parameters and consequently different spatial resolutions. Such heterogenous CT data resemble daily clinical practice and also show the robustness of CTBMA.

## 5.6 FUTURE RESEARCH

### 5.6.1 Within current data

In future analyses of the current project, an additional seven patients could be added if they complete follow-up. Data collection on these patients is expected to end around July 2022. With these additional seven patients, the required sample size for rotation measurements will not yet be met but it will provide a better representation of the population.

Also, in addition to migration of the tibial component the migration of the femoral component should be analyzed. In the current analysis, we solely focused on tibial component because the Dutch arthroplasty register (LROI) suggest that tibial components migrate more often than femoral components [53]. Segmentation of the femoral components could be more challenging due to the more present artifacts compared to tibial components.

Furthermore, it would be interesting to see if limits of agreement differ for the two different tibial designs of this study, since different designs could result in different artifacts potentially affecting the accessibility of segmentation. This was outside the scope of the current study.

Lastly, the robustness of the method could be tested with a sensitivity analysis. A sensitivity analysis could be used to detect the influences of certain input parameters to the output of the method. This analysis can be used to see which parameter in CTBMA should be further optimized.

### **5.6.2 Future studies**

First of all, future studies should investigate the applicability of CTBMA for overall use of quality control of new implants. Including implant designs with other material properties and other joints. Further external validation of CTBMA is advised. Also, the agreement between CTBMA and RSA in larger sample sizes and larger variations in migration measurements. The latter could be achieved by imaging direct postoperative after TKA.

Furthermore, more constant use of a CT protocol is needed to achieve more consistency in CT images. The spatial resolution of CT images can be improved by limiting the size of the field of view, meaning that the field of view only contains the knee and nothing more. This will improve pixel size and is expected to improve results of CTBMA, although our study did not provide prove for a better agreement between CTBMA and RSA when the spatial resolution of the images were better.

Future research should also include the clinical precision of the method by assessing double examinations, similar to RSA.

### **5.6.3 Possible improvements of CTBMA**

A suggestion to improve CTBMA is to include measurement of maximal total point of motion (MTPM). MTPM is the TT of a point on the implant which moved the most [6] and is used to classify early migration when the value exceeds 0.5 mm at six months postoperatively [7]. Hence, this will be an improvement to use in clinical studies comparing new implant designs.

Another improvement would be to reduce manual steps in the method to improve objectiveness of method. Some options are proposed earlier such as automated segmentation and model-based CTBMA.

Finally, a formal study reporting the *in vitro* accuracy and precision results of CTBMA should be published so that the scientific community can enhance and build upon these results.

## 6. CONCLUSION

In this work, CT-based migration analysis (CTBMA) was investigated as alternative to roentgen stereophotogrammetric analysis (RSA) for the migration measurement in total knee arthroplasty (TKA). This was the first study to investigate CTBMA for tibial components in TKA. In a prospective study, tibial component migration was measured between one year (YR1) and five years (YR5) postoperatively, both with CTBMA and model-based RSA (currently the gold standard). For CTBMA, masks of the tibial component and tibia (bone) were defined by manual segmentation in the CT image of YR1. The underlying voxel intensities of these masks were matched on the CT image of YR5 using image registration. This was performed by means of a graphical user interface, which allows visual verification of the image registration. Migration is defined as a shift in position of the prosthesis over time. The derivation of the coordinate transformation for the calculation of migration is given.

The displacement of tibial component relative to the tibia was measured in TKA for seventeen patients. These migration measurements were compared to RSA using Bland-Altman plots which provided limits of agreement. The limits of agreement,  $[-0.46 \text{ mm to } 0.33 \text{ mm}]$  for total translation and  $[-0.88^\circ \text{ to } 0.64^\circ]$  for total rotation, were within the pre-defined values of  $\pm 0.5 \text{ mm}$  and  $\pm 0.8^\circ$  respectively. These results indicate that CTBMA is comparable to RSA for migration measurement of tibial components in TKA. Hence, CTBMA could be considered as a promising marker-free alternative method for evaluation of tibial component migration in TKA in hospitals with a similar CT scanner.

In future research, the accuracy, clinical precision and robustness of CTBMA could be evaluated. Future studies could include analysis of other joints, implants and designs, as well as further external validation to indicate the applicability of CTBMA.

## REFERENCES

- [1] LROI, "Landelijke registratie orthopedische implantaten: Jaarraport 2020," p. 6, 2020.
- [2] R. Otten, P. M. van Roermund, and H. S. J. Picavet, "Trends in the number of knee and hip arthroplasties: considerably more knee and hip prostheses due to osteoarthritis in 2030," *Ned. Tijdschr. Geneesk.*, vol. 154, no. 20, pp. 1–7, 2010.
- [3] J. T. Evans, R. W. Walker, J. P. Evans, A. W. Blom, A. Sayers, and M. R. Whitehouse, "How long does a knee replacement last? A systematic review and meta-analysis of case series and national registry reports with more than 15 years of follow-up," *Lancet*, vol. 393, no. 10172, pp. 655–663, 2019, doi: 10.1016/s0140-6736(18)32531-5.
- [4] "National Joint Registry for England Wales Northern Ireland and the Isle of Man. 18th Annual Report 2021," *National Joint Registry | 18th Annual Report, 2021*. [www.njrcentre.org.uk](http://www.njrcentre.org.uk) (accessed May 06, 2022).
- [5] M. Sundfeldt, L. V. Carlsson, C. B. Johansson, P. Thomsen, and C. Gretzer, "Aseptic loosening, not only a question of wear: A review of different theories," *New Pub Med. Journals Sweden*, vol. 77, no. 2, pp. 177–197, Apr. 2009, doi: 10.1080/17453670610045902.
- [6] L. Ryd *et al.*, "Roentgen stereophotogrammetric analysis as a predictor of mechanical loosening of knee prostheses," *J. Bone Jt. Surg. - Ser. B*, vol. 77, no. 3, pp. 377–383, 1995, doi: 10.1302/0301-620x.77b3.7744919.
- [7] B. G. Pijls, J. W. M. Plevier, and R. G. H. H. Nelissen, "RSA migration of total knee replacements: A systematic review and meta-analysis," *Acta Orthop.*, vol. 89, no. 3, pp. 320–328, 2018, doi: 10.1080/17453674.2018.1443635.
- [8] B. G. Pijls *et al.*, "Early proximal migration of cups is associated with late revision in THA: A systematic review and meta-analysis of 26 RSA studies and 49 survival studies," *Acta Orthop.*, vol. 83, no. 6, pp. 583–591, 2012, doi: 10.3109/17453674.2012.745353.
- [9] B. Mjöberg, "Is early migration enough to explain late clinical loosening of hip prostheses?," *EFORT Open Rev.*, vol. 5, no. 2, pp. 113–117, 2020, doi: 10.1302/2058-5241.5.190014.
- [10] E. R. Valstar, H. A. Vrooman, S. Toksvig-Larsen, L. Ryd, and R. G. H. H. Nelissen, "Digital automated RSA compared to manually operated RSA," *J. Biomech.*, vol. 33, no. 12, pp. 1593–1599, 2000, doi: 10.1016/S0021-9290(00)00138-X.
- [11] E. R. Valstar, R. Gill, L. Ryd, G. Flivik, N. Börlin, and J. Kärrholm, "Guidelines for standardization of radiostereometry (RSA) of implants," *Acta Orthop.*, vol. 76, no. 4, pp. 563–572, 2005, doi: 10.1080/17453670510041574.
- [12] G. Selvik, "Roentgen stereophotogrammetry. A method for the study of the kinematics of the skeletal system," *Acta Orthop. Scand. Suppl.*, vol. 232, pp. 1–51, 1989.
- [13] J. Kärrholm, B. Borssen, G. Lowenhielm, and F. Snorrason, "Does early micromotion of femoral stem prostheses matter? 4-7-year stereoradiographic follow-up of 84 cemented prostheses," *J. Bone Jt. Surg. - Ser. B*, vol. 76, no. 6, pp. 912–917, 1994, doi: 10.1302/0301-620x.76b6.7983118.
- [14] H. Malchau, "Introducing new technology: A stepwise algorithm," *Spine (Phila. Pa. 1976)*, vol. 25, no. 3, p. 285, 2000, doi: 10.1097/00007632-200002010-00004.
- [15] R. G. H. H. Nelissen, B. G. Pijls, and J. Kärrholm, "RSA and Registries: The Quest for Phased Introduction of New Implants," *J. Bone Jt. Surg.*, vol. 3, pp. 62–65, 2011.
- [16] J. Kärrholm, R. H. S. Gill, and E. R. Valstar, "The history and future of radiostereometric analysis," *Clin. Orthop. Relat. Res.*, no. 448, pp. 10–21, 2006, doi: 10.1097/01.blo.0000224001.95141.fe.
- [17] S. Hasan, P. J. Marang-van de Mheen, B. L. Kaptein, R. G. H. H. Nelissen, and B. G. Pijls, "RSA-tested TKA Implants on Average Have Lower Mean 10-year Revision Rates Than Non-RSA-tested Designs," *Clin. Orthop. Relat. Res.*, vol. 478, no. 6, pp. 1232–1241, 2020, doi:

10.1097/CORR.0000000000001209.

- [18] J. Kärrholm, "Roentgen stereophotogrammetry: Review of orthopedic applications," *Acta Orthop.*, vol. 60, no. 4, pp. 491–503, 1989, doi: 10.3109/17453678909149328.
- [19] B. L. Kaptein, E. R. Valstar, B. C. Stoel, H. C. Reiber, and R. G. Nelissen, "Clinical validation of model-based RSA for a total knee prosthesis," *Clin. Orthop. Relat. Res.*, no. 464, pp. 205–209, 2007, doi: 10.1097/BLO.0b013e3181571aa5.
- [20] E. R. Valstar, F. W. De Jong, H. A. Vrooman, P. M. Rozing, and J. H. C. Reiber, "Model-based Roentgen stereophotogrammetry of orthopaedic implants," *J. Biomech.*, vol. 34, no. 6, pp. 715–722, 2001, doi: 10.1016/S0021-9290(01)00028-8.
- [21] International Standard ISO 16087:2013, "Implants for surgery - Roentgen stereophotogrammetric analysis for the assessment of migration of orthopaedic implants," vol. 2013, 2013.
- [22] J. Ranstam, L. Ryd, and I. Onsten, "Erratum: Accurate accuracy assessment: Review of basic principles (*Acta Orthopaedica Scandinavica* (1999) 70 4 (319-321))," *Acta Orthop. Scand.*, vol. 71, no. 1, pp. 106–108, 2000, doi: 10.1080/00016470052944017.
- [23] I. Önsten, A. Berzins, S. Shott, and D. R. Sumner, "Accuracy and precision of radiostereometric analysis in the measurement of THR femoral component translations: Human and canine in vitro models," *J. Orthop. Res.*, vol. 19, no. 6, pp. 1162–1167, 2001, doi: 10.1016/S0736-0266(01)00039-0.
- [24] L. A. Koster, J. E. Meinardi, B. L. Kaptein, E. Van der Linden-Van der Zwaag, and R. G. H. H. Nelissen, "Two-year RSA migration results of symmetrical and asymmetrical tibial components in total knee arthroplasty: a randomized controlled trial," *Bone Joint J.*, vol. 103-B, no. 5, pp. 855–863, 2021, doi: 10.1302/0301-620X.103B5.BJJ-2020-1575.R2.
- [25] B. L. Kaptein, E. R. Valstar, B. C. Stoel, P. M. Rozing, and J. H. C. Reiber, "A new model-based RSA method validated using CAD models and models from reversed engineering," *J. Biomech.*, vol. 36, no. 6, pp. 873–882, 2003, doi: 10.1016/S0021-9290(03)00002-2.
- [26] J. Ranstam, "Methodological Note: Accuracy, precision, and validity," *Acta radiol.*, 2008, doi: 10.1080/02841850701772706.
- [27] LUMC, "Model-based Roentgen Stereophotogrammetric Analysis of Orthopaedic Implants." <https://www.lumc.nl/org/radiologie/research/LKEB/PMO/904021121292222/> (accessed Nov. 01, 2021).
- [28] L. Olivecrona *et al.*, "Acetabular Component Migration In Total Hip Arthroplasty Using CT and A Semiautomated Program for Volume Merging," *Acta radiol.*, vol. 43, pp. 517–527, 2002, doi: 10.1034/j.1600-0455.2003.00086.x.
- [29] H. Olivecrona *et al.*, "Acta Orthopaedica A new technique for diagnosis of acetabular cup loosening using computed tomography: Preliminary experience in 10 patients A new technique for diagnosis of acetabular cup loosening using computed tomography Preliminary experience in 10 patients," *Acta Orthop.*, vol. 79, no. 3, pp. 346–353, 2008, doi: 10.1080/17453670710015247.
- [30] L. Olivecrona, H. Olivecrona, L. Weidenhielm, M. E. Noz, G. Q. Maguire, and M. P. Zeleznik, "Model studies on acetabular component migration in total hip arthroplasty using CT and a semiautomated program for volume merging," *Acta radiol.*, vol. 44, no. 4, pp. 419–429, 2003, doi: 10.1034/j.1600-0455.2003.00086.x.
- [31] T. Scheerlinck, M. Polfliet, R. Deklerck, G. Van Gompel, N. Buls, and J. Vandemeulebroucke, "Development and validation of an automated and marker-free CT-based spatial analysis method (CTSA) for assessment of femoral hip implant migration In vitro accuracy and precision comparable to that of radiostereometric analysis (RSA)," *Acta Orthop.*, vol. 87, no. 2, pp. 139–145, 2016, doi: 10.3109/17453674.2015.1123569.
- [32] C. Brodén, H. Olivecrona, G. Q. Maguire, M. E. Noz, M. P. Zeleznik, and O. Sköldenberg, "Accuracy and Precision of Three-Dimensional Low Dose CT Compared to Standard RSA in

- Acetabular Cups: An Experimental Study," *Biomed Res. Int.*, vol. 2016, 2016, doi: 10.1155/2016/5909741.
- [33] V. Otten, G. Q. Maguire, M. E. Noz, M. P. Zeleznik, K. G. Nilsson, and H. Olivecrona, "Are CT Scans a Satisfactory Substitute for the Follow-Up of RSA Migration Studies of Uncemented Cups? A Comparison of RSA Double Examinations and CT Datasets of 46 Total Hip Arthroplasties," *Biomed Res. Int.*, vol. 2017, 2017, doi: 10.1155/2017/3681458.
- [34] C. Brodén *et al.*, "Low-dose CT-based implant motion analysis is a precise tool for early migration measurements of hip cups: a clinical study of 24 patients," *Acta Orthop.*, vol. 91, no. 3, pp. 260–265, 2020, doi: 10.1080/17453674.2020.1725345.
- [35] C. Brodén, O. Sandberg, H. Olivecrona, R. Emery, and O. Sköldenberg, "Precision of CT-based micromotion analysis is comparable to radiostereometry for early migration measurements in cemented acetabular cups," *Acta Orthop.*, vol. 92, no. 4, pp. 419–423, 2021, doi: 10.1080/17453674.2021.1906082.
- [36] M. van Eijnatten, R. van Dijk, J. Dobbe, G. Streekstra, J. Koivisto, and J. Wolff, "CT image segmentation methods for bone used in medical additive manufacturing," *Med. Eng. Phys.*, vol. 51, pp. 6–16, 2018, doi: 10.1016/j.medengphy.2017.10.008.
- [37] J. Van den Broeck, E. Vereecke, R. Wirix-Speetjens, and J. Vander Sloten, "Segmentation accuracy of long bones," *Med. Eng. Phys.*, vol. 36, no. 7, pp. 949–953, 2014, doi: 10.1016/j.medengphy.2014.03.016.
- [38] S. Klein, M. Staring, K. Murphy, M. A. Viergever, and J. P. W. Pluim, "Elastix: A toolbox for intensity-based medical image registration," *IEEE Trans. Med. Imaging*, vol. 29, no. 1, pp. 196–205, Jan. 2010, doi: 10.1109/TMI.2009.2035616.
- [39] S. Klein and M. Staring, "The Elastix Manual," 2019. <https://elastix.lumc.nl/doxygen/index.html> (accessed Mar. 23, 2022).
- [40] D. Eberly, "Euler angle formulas," *Geometric Tools*, 2020. <http://www.geometrictools.com/Documentation/EulerAngles.pdf> (accessed Jun. 19, 2022).
- [41] J. M. Bland and D. G. Altman, "Comparing methods of measurement : why plotting difference against standard method is misleading," *Clin. Lab. Haematol.*, vol. 346, pp. 1085–1087, 1995.
- [42] J. M. Bland and D. G. Altman, "Statistical methods for assessing agreement between two methods of clinical measurement," *Lancet*, vol. 327, no. 8476, pp. 307–310, Feb. 1986, doi: 10.1016/S0140-6736(86)90837-8.
- [43] D. Giavarina, "Lessons in biostatistics. Understanding Bland Altman analysis," *Biochem. medica*, vol. 25, no. 2, pp. 141–151, 2015, doi: 10.11613/BM.2015.015.
- [44] K. T. van Hamersveld, P. J. Marang-van de Mheen, L. A. Koster, R. G. H. H. Nelissen, S. Toksvig-Larsen, and B. L. Kaptein, "Marker-based versus model-based radiostereometric analysis of total knee arthroplasty migration: a reanalysis with comparable mean outcomes despite distinct types of measurement error," *Acta Orthop.*, vol. 90, no. 4, pp. 366–372, Jul. 2019, doi: 10.1080/17453674.2019.1605692.
- [45] C. Hurschler, F. Seehaus, J. Emmerich, B. L. Kaptein, and H. Windhagen, "Comparison of the Model-Based and Marker-Based Roentgen Stereophotogrammetry Methods in a Typical Clinical Setting," *J. Arthroplasty*, vol. 24, no. 4, pp. 594–606, 2009, doi: 10.1016/j.arth.2008.02.004.
- [46] A. Gudnason, G. Adalberth, K. G. Nilsson, and N. P. Hailer, "Tibial component rotation around the transverse axis measured by radiostereometry predicts aseptic loosening better than maximal total point motion: A follow-up of 116 total knee arthroplasties after at least 15 years," *Acta Orthop.*, vol. 88, no. 3, pp. 282–287, 2017, doi: 10.1080/17453674.2017.1297001.
- [47] F. F. Schröder *et al.*, "Low-field magnetic resonance imaging offers potential for measuring tibial component migration," *J. Exp. Orthop.*, vol. 5, no. 1, 2018, doi: 10.1186/s40634-017-0116-2.

- [48] C. Brodén *et al.*, “Accuracy and precision of a CT method for assessing migration in shoulder arthroplasty: an experimental study,” *Acta radiol.*, vol. 61, no. 6, pp. 776–782, 2020, doi: 10.1177/0284185119882659.
- [49] B. G. Pijls and R. G. H. H. Nelissen, “The era of phased introduction of new implants,” *Bone Jt. Res.*, vol. 5, no. 6, pp. 215–217, 2016, doi: 10.1302/2046-3758.56.2000653.
- [50] H. G. Menzel and J. Harrison, “Effective dose: A radiation protection quantity,” *Ann. ICRP*, vol. 41, no. 3–4, pp. 117–123, 2012, doi: 10.1016/j.icrp.2012.06.022.
- [51] D. Biswas, J. E. Bible, M. Bohan, A. K. Simpson, P. G. Whang, and J. N. Grauer, “Radiation exposure from musculoskeletal computerized tomographic scans,” *J. Bone Jt. Surg. - Ser. A*, vol. 91, no. 8, pp. 1882–1889, 2009, doi: 10.2106/JBJS.H.01199.
- [52] G. J. Teeuwisse W, Berting R, “Stralenbelasting bij orthopedische radiologie.,” *Gamma*, vol. 8/9, pp. 197–200, 1998.
- [53] Landelijke Registratie Orthopedische Implantaten (LROI), “Trend (proportion [%] per year) in reasons for revision in patients who underwent a knee revision arthroplasty in the Netherlands in 2014-2020.” <https://www.lroi-report.nl/knee/knee-revision-arthroplasty/reasons-for-revision/> (accessed Mar. 29, 2022).





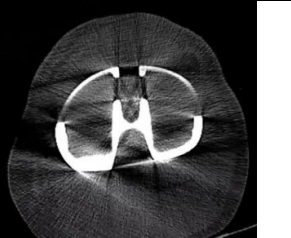
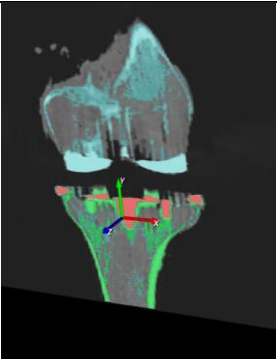
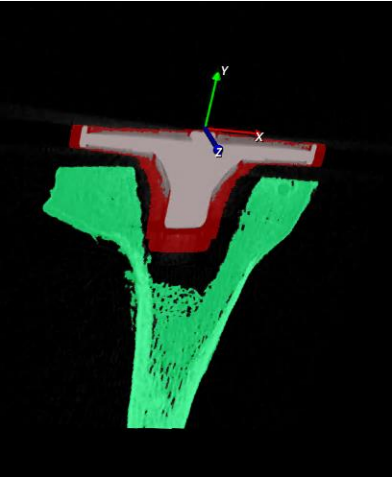
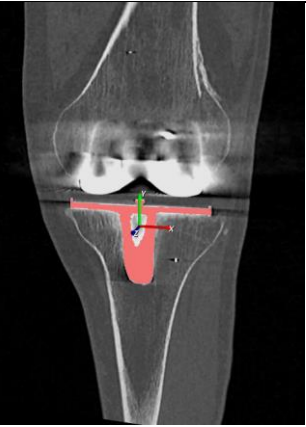
# APPENDIX A: DEVELOPMENT OF METHOD

This appendix covers the development of the methodology of CT-based migration analysis (CTBMA) used for the clinical study. These experiments are performed on three different datasets.

An overview of the datasets and accompanying experiments are given in **table 6**. All three datasets consist of CT images:

- Dataset A represents a cadaveric bone with cemented total knee prosthesis for zero-migration measurement. This dataset is used for the development of the segmentation algorithm, to closely represent clinical data, with (known) zero-migration influences.
- Datasets B represent the micromanipulator which can apply a translation and rotation to the attached tibial component. This dataset is used to determine the accuracy of the segmentation algorithm, while applying a known displacement and rotation of the prosthesis with respect to the tibia. The dataset is also used to evaluate the accuracy by varying segmentation algorithm parameters.
- Dataset C represents clinical CT images of patients knee after total knee replacement. This dataset is used to determine the order of registration in the data used for the clinical study. Furthermore this datasets represents data from clinical practice.

Table 6: overview of three datasets A, B and C. The second row of images show the images as seen in the CTRSA-software.

A	B	C
		
		
<p>Cadaveric human bone + cemented total knee prosthesis</p>	<p>Cadaveric human bone + uncemented tibial component attached to micromanipulator</p>	<p>Patients: one and five years after total knee prosthesis</p>
<p>Experiment 1 + 2</p>	<p>Experiment 3 + 4</p>	<p>Experiment 5 + 6</p>

In this appendix, the experiments on datasets A,B and C are described. Each experiment contains the following structure: aim, hypothesis, method, results, conclusions and discussions. These experiments are summarized in **table 7**.

Table 7: Experiments conducted for the development of the method

Exp.	Dataset	Aim	Hypothesis	Altered parameters
1	A	Try out segmentation method and determine segmentation algorithm of prosthesis	The combination of region grow with morphological opening and closing results in a visual accurate mask	Segmentation
2	A	Verification of calculation of migration	Migration measurements approaches zero	Segmentation
3	B	Determine amount of pixel dilation for the segmentation algorithm	The migration is more accurate when edges are included in segmentation (thus pixel dilation is better than normal / erode)	Segmentation
4	B	Order of registration	Using prosthesis registration as starting point for bone registration results in less calculation time and more accurate results	Registration
5	C	Determine align mask	Initial alignment of CT images is similar for different align masks	Segmentation & registration
6	C	Order of registration	Using prosthesis registration as starting point for bone registration results in migration values closer to zero	Registration

All these experiments contributed to the method of CTBMA as used in **chapter 3** of this master thesis.

The pipeline of CTBMA is shown in **figure 11**. In this image, the flow of information is from left to right. The method exists of four steps: data acquisition, mask defining, registration and calculation of migration. Mask defining using segmentation is performed in Mimics, a software toolbox of Materialise, which offers a wide range of tools to segment the anatomy to create masks. A mask is a group of pixels with the same label. Three masks were obtained by segmentation: an align mask, a mask of the bone, and a mask of the prosthesis. The registration is done based on the underlying voxel values of these masks, using open software Elastix. The registration is performed with a novel in-house build graphical user interface (CTRSA-software, Python v3.9.7),<sup>1</sup>. In this graphical user interface, three steps are needed for image registration: the initial alignment (align), the alignment of bone and the alignment of prosthesis. The align registration is always used first. The registration of bone and prosthesis are based on this align (using the align registration as starting point) unless specified otherwise.

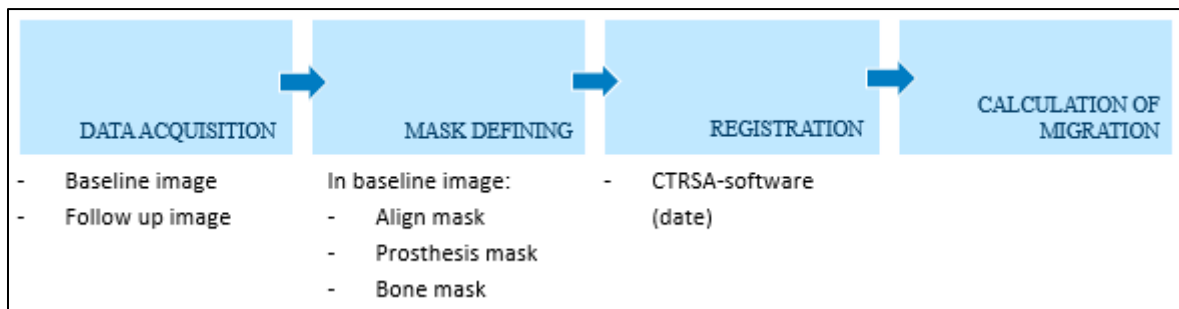


Figure 11: Pipeline of CTBMA consisting of four steps: data acquisition, mask defining, registration and calculation of migration. The information provided by each step corresponds to the information provided by the experiments.

<sup>1</sup> The CTRSA-software does not contain version number, therefore the date of use during experiments was added. To indicate which version was used. See end of appendix A for comparison between an older and newer version of CTRSA-software.

## DATASET A: CADAVERIC BONE

**Set-up:** Two cadaveric tibia bones of human origin with cemented tibial component in TKA. The tibial component was firmly attached to the bone and therefore, theoretically, the migration will approach zero displacement. The set-up was moved and removed from the CT scanner so that the position was changed between each CT scan.

**CT data:** There are 5 CT scans available for each cadaver (2485 and 2509) named: SEMAR\_S01, SEMAR\_S02, SEMAR\_S03, SEMAR\_S04 and SEMAR\_S05. Data acquisition processing was equal in all CT volumes, **see table 8**.

Table 8: Overview of CT parameters of CT images used in dataset A.

Parameter	Setting
Scanner	Toshiba, Aquilion ONE
Slice Thickness (mm)	0.5
Pixel Spacing (mm\mm)	0.976\0.976
Number of Frames	640
Rows	512
Columns	512
Convolution Kernel	FC30 <sup>2</sup>
CT tube voltage (kVp)	120
Xray Tube Current (mA)	30
Scan Options	VOLUME_CT
Data collection Diameter	500
Focal spot	0.9\0.8

### Experiment 1: Try out segmentation method

**Aim:** Define the mask of tibial component and tibia.

**Hypothesis:** The combination of region grow with morphological opening and closing results in a visual accurate mask.

**Method:** Compare the six different segmentation algorithms on required operator time and feasibility of the aim. The segmentation mask is visually inspected, and the performance of segmentation is qualitatively assessed. All segmentations are performed manually.

- Data: Kadaver2509\_LeftKnee-S01\_SEMAR.
- Segmentation:
  - o 5x different mask of tibia component of prosthesis and corresponding tibia bone.
  - o Segmentation algorithm for prosthesis:
    1. Threshold to include the prosthesis
      - a. Small or large threshold interval, **see figure 12**.
    2. Region grow (select tibia component)
      - a. 6 or 26 connectivity? 6 connectivity (neighboring faced voxels) and 26 connectivity (neighboring faces, nodes and vertices)
    3. Morphological opening/closing ? (one part, filled)
      - a. morphological opening (erode followed by an open) and closing (dilate followed by an open): 1 or 2 pixels?
  - o Segmentation algorithm for bone:
    4. Threshold to include bone.
    5. Region grow (select tibia bone).
    6. Boolean operation to extract prosthesis from bone (subtraction = bone mask minus prosthesis mask).
- Registration: not used in this experiment.

### Results:

A custom threshold (segmentation in step 1a in method above) is set based on the histogram of the CT image, see **figure 12** where the left image represent a large threshold and the right image represents a small threshold.

<sup>2</sup> FC30 refers to a Toshiba convolution kernel used in image reconstruction.

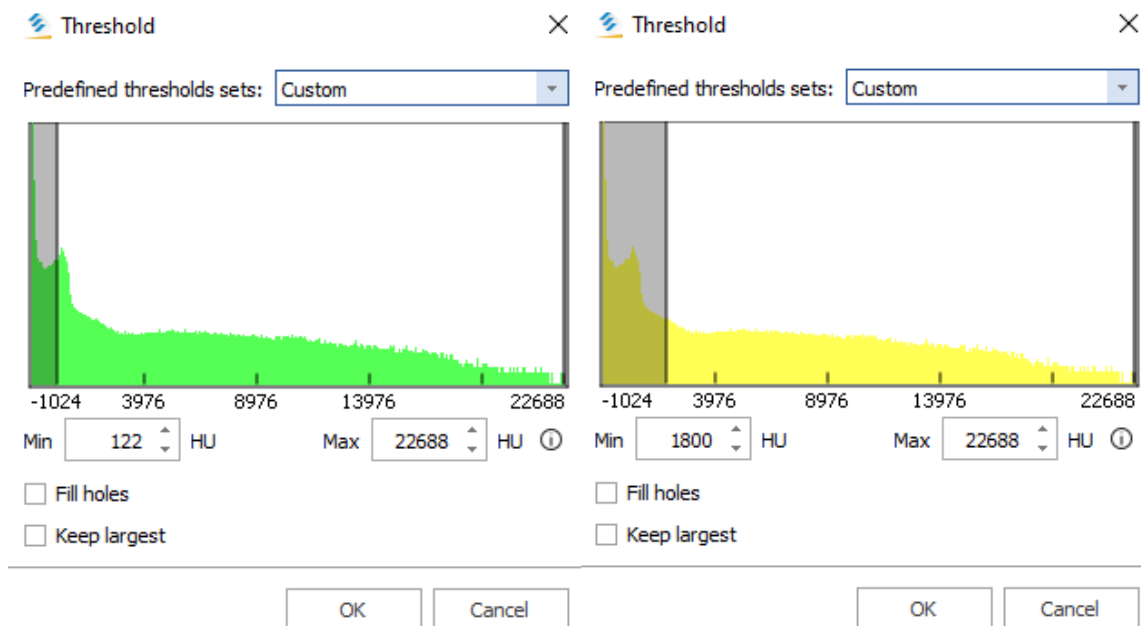


Figure 12: Example of user interface in Mimics for thresholding. An example of a large threshold (left) and a small threshold (right) for defining the prosthesis mask.

The multiple steps in the segmentation algorithm with resulting mask of the prosthesis are seen in **table 9**. In this table, the defining of the prosthesis mask is visualised step by step using the segmentation tools of Mimics.

Table 9: Segmentation algorithm. Flow of segmentation steps is from left to right. Abbreviations: LT = large threshold, RG = region grow, 6c = 6 connectivity, O = open, px = pixel

Start >>>	Threshold	Region grow	Morphological opening & closing 1 pixel	Region grow	Morphological opening & closing 2 pixels	Region grow
Name	Prosthesis_LT	Prosthesis_LT_R G6c	Prosthesis_LT_O_C1 ose	Prosthesis_Tibia_M ask	PTM_O_Close_2px	PTM_RG

Required operator time for segmentation of PTM\_RG:  $\pm 23$  min. The processing time in Mimics is negligible with respect to the required operator time. Another mask was made based on a small threshold to visually compare these masks see figure 13. Also, a difference in mask was seen when region grow was performed with 6 connectivity (neighboring faced voxels) and 26 connectivity (neighboring faces, nodes and vertices) to the selected voxel and those voxels which are connected to it, see figure 14. Furthermore, morphological opening (erode followed by an open) and closing (dilate followed by an open) of 1 pixels and 2 pixels results in different masks, mainly the affecting the tibia plateau, see figure 15. All objects of prosthesis and corresponding bone are seen in figure 16.

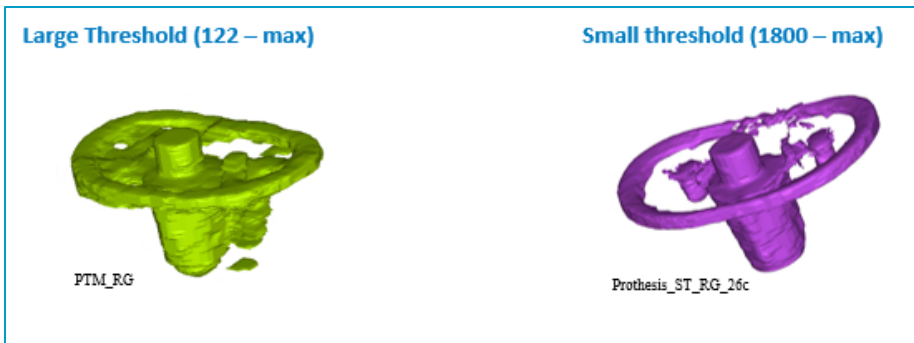


Figure 13: Visual example of final mask when as first step a large threshold (left tibia component) and small threshold (right tibia component) is used.

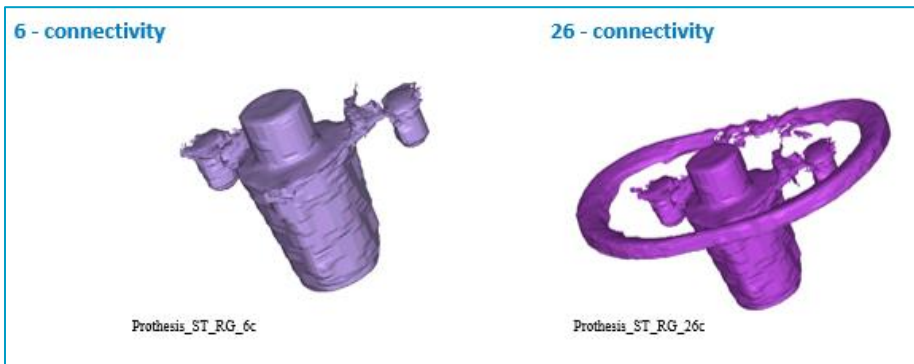


Figure 14: Visual example of difference in the masks when 6 connectivity (left tibia component) and 26 connectivity (right tibia component) is used for region grow.

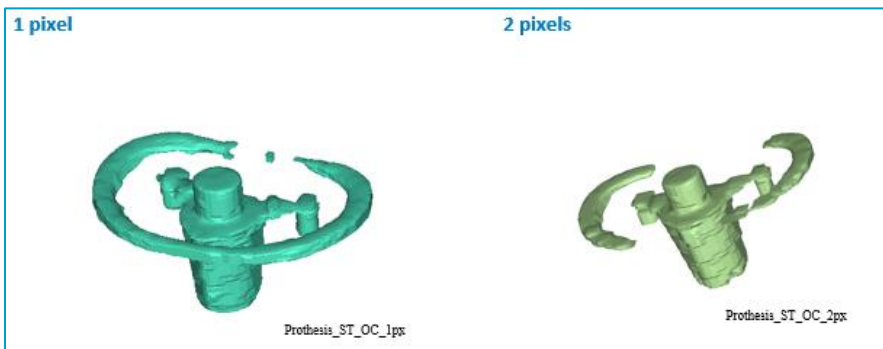


Figure 15: Visual example of the difference in masks when 1 pixel (left) and 2 pixel (right) is used for morphological open and close.

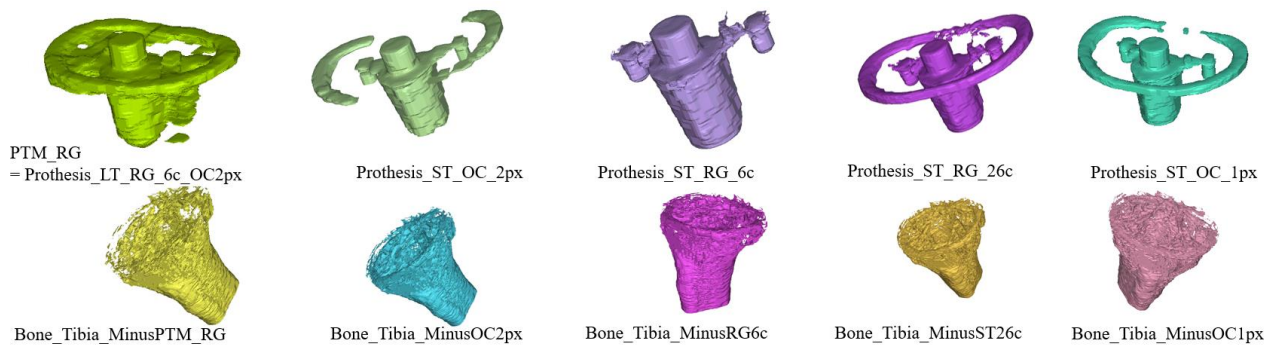


Figure 16: The six different masks of the prosthesis with corresponding bone masks.

## Conclusion and discussion:

- The CT image contains metal artifacts resulting in visually inaccurate tibia plateau in all masks.
- A threshold + region grow when using a large threshold does not result in a decent segmentation by visual inspection, since the tibia and femur are still included. Therefore, additional segmentation steps are required. A smaller threshold seems to result in a better representation of the tibial component and costs less operator time due to less subsequent manual steps.
- A Boolean operation (subtraction, bone mask minus prosthesis mask) to exclude prosthesis mask from bone mask works sufficiently by visual inspection.
- The different steps of segmentation result in different masks of prosthesis and bone, but does this result in different migration measurement? This will be investigated in experiment 2.

## Experiment 2: Migration measurement of zero-migration with 6 different masks

**Aim:** Calculate the migration of the prosthesis relative to the bone for six different masks with zero-migration.

**Hypothesis:** For different types of masks, the migration still approaches zero in translation and rotation.

**Method:** The segmentation masks differ for prosthesis and bone in this experiment.

- Data:
  - o Baseline image: Kadaver2509\_LeftKnee-S01\_SEMAR
  - o Follow-up image: Kadaver2509\_LeftKnee S02\_SEMAR - S05\_SEMAR
- Segmentation:
  - o In baseline image: 6x different mask of tibia component of prosthesis and corresponding tibia bone from experiment 1
  - o Segmentation algorithm for prosthesis:

Experiment	Segmentation algorithm
2.0	Large threshold, RG 6c, OC 1 px, RG 6c, OC 2 px
2.1	Small threshold, RG 26c, OC 2 pixel
2.2	Small threshold, RG 6c
2.3	Small threshold, RG 26c
2.4	Small threshold, RG 26c, OC 1 px
2.5	Small threshold, RG 6c, manual edit to make it symmetrical around Y-axis
Abbreviations: LT = large threshold, RG = region grow, 6c = 6 connectivity, O = open, C = close px = pixel	

- Registration:
  - o CTRSA-software (date: 02-12-2021)

## Results:

The migration of prosthesis relative to the bone results of the six different masks in four follow-up moments are seen in **figure 17 and 18**. For masks 2.0 until and including 2.4 the translations in all 4 follow-up moments are between -0.1 and 0.1 mm in all directions. The rotations for masks 2.0-2.4 are between -0.1 and 0.1 degrees except for  $R_y$ , which corresponds to rotations around the inferior-superior axis. The symmetrical mask of 2.5 results in the largest value of -2.21 degrees for  $R_y$ .

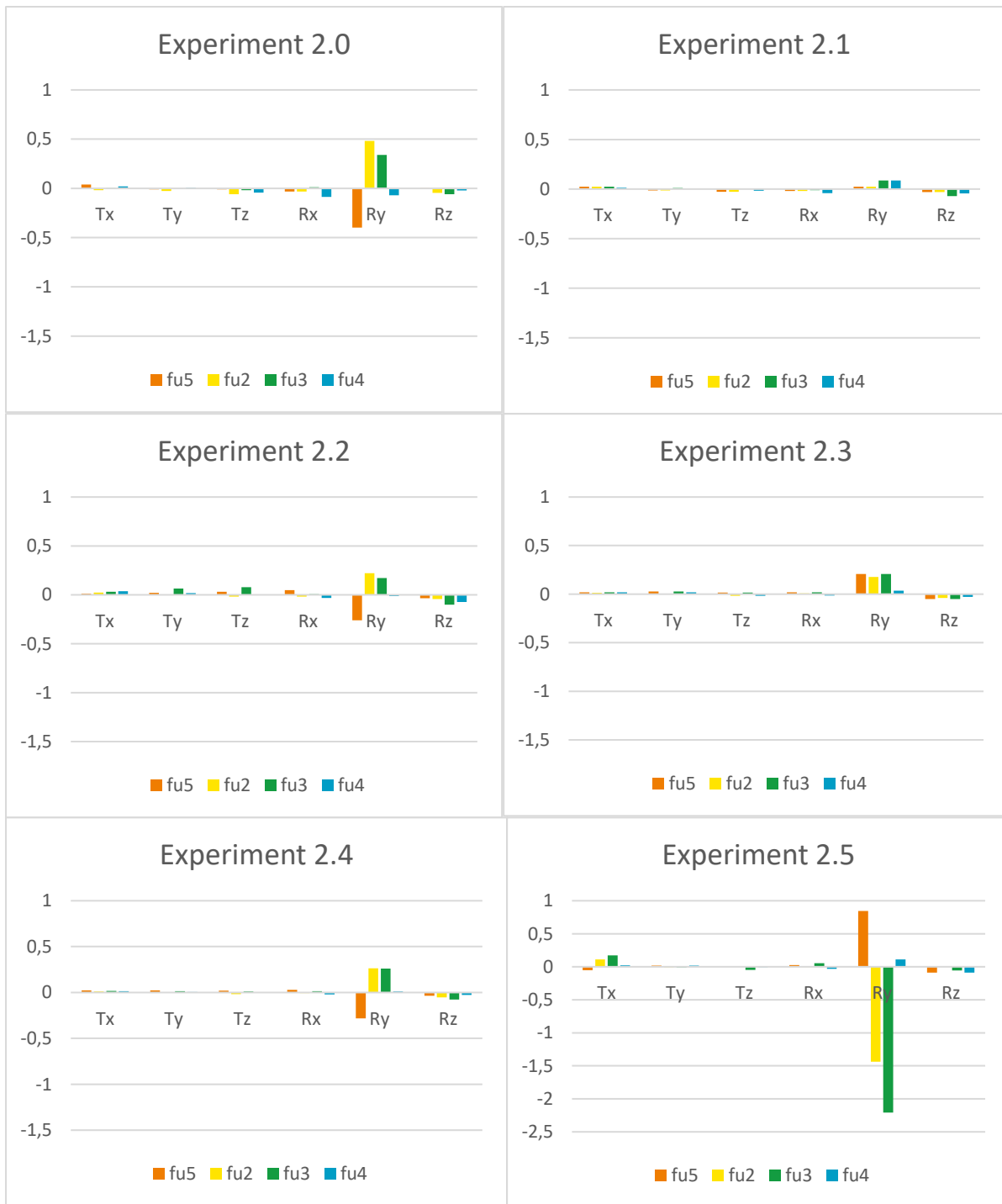


Figure 17: Migration results for six different tibia masks and corresponding mask of tibia bone in four different follow-up fu2-fu5 (n = 4). Translations (mm) and rotations (degrees) measurements are given in x, y and z direction. Abbreviations: fu = follow-up.



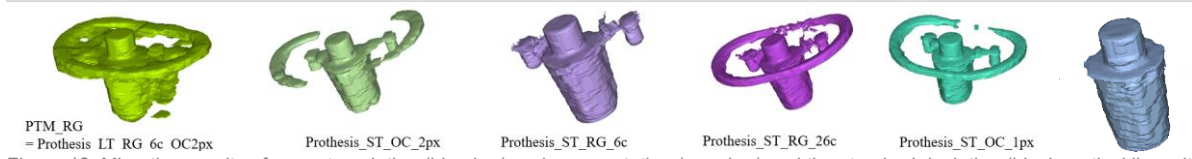
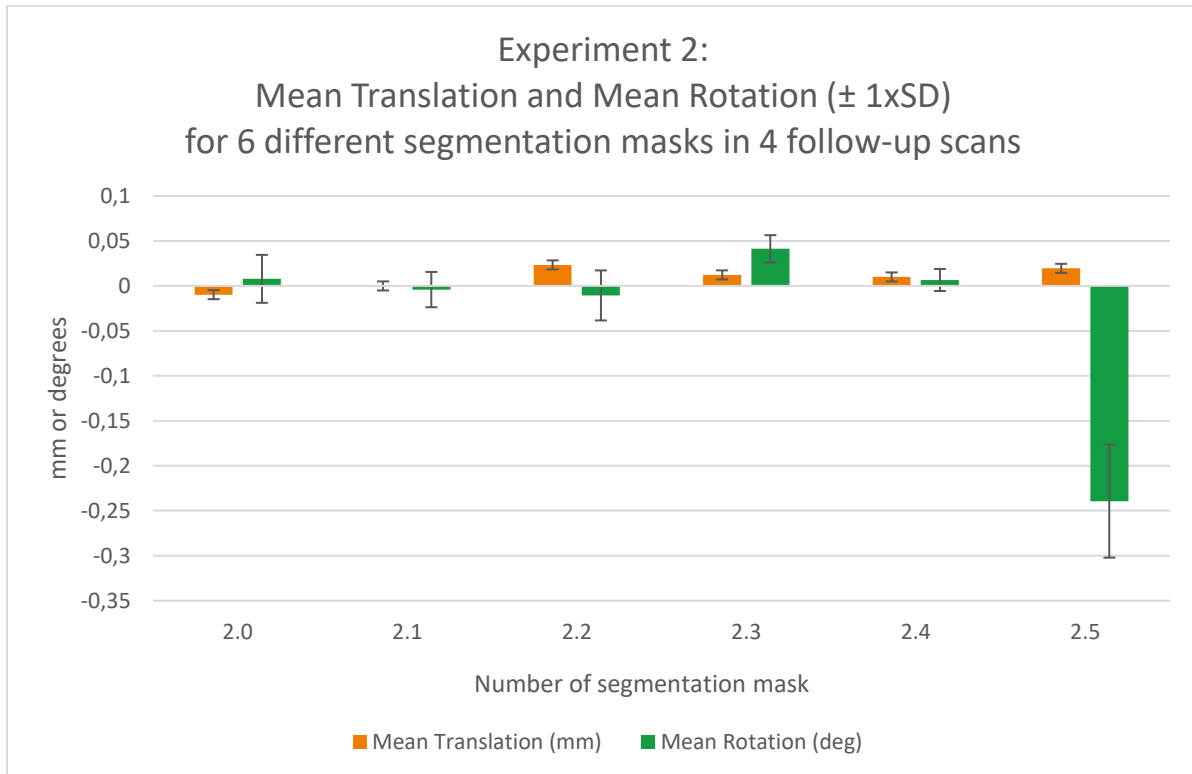


Figure 18: Migration results of mean translation (blue bar) and mean rotation (grey bar) and the standard deviation (black vertical line with cap) for six different masks (2.0 - 2.5) in four different follow-up scans ( $n = 4$ ). The number of segmentation mask correspond with the image of the prosthesis mask below. The corresponding mask of tibia bone is not visible in this figure.

The mean  $\pm$  SD of migration for the six different masks are seen in **table 10**. The translations are  $< 0.05$  mm in all directions for all masks except for mask number 2.5. The rotations for all masks but 2.5 are  $< 0.05^\circ$  around the X-axis and Z-axis, but not around the Y-axis. Depending on the type of mask the mean  $\pm$  SD of  $R_y$ , varies between  $0.04^\circ$  and  $1.4^\circ$ .

**Conclusion:**

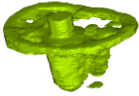
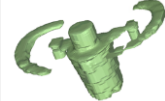
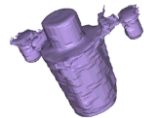
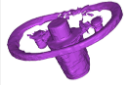
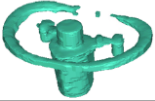

- The mean  $\pm$  SD of zero-migration measurement is in the same order for all masks as long as the mask is asymmetrical (thus the tibia plateau needs to be included in the mask).

**Discussion:**

- The rotation around the Y-axis ( $R_y$ ), which corresponds to rotations around the inferior-superior axis varies between the different masks.
- The values for  $R_y$  of mask number 2.5 is explained by the mask being symmetrical in Y-axis. This rotation symmetry is difficult for correct alignment
- This experiment contains one type of prosthesis, one type of CT scan, and only 4 follow-up images, therefore the results should be interpreted with care.
- For precision measurement  $1xSD$  could be low (only 53% of data is included assuming data is normally distributed)
- The segmentation & registration part of method are linked and influence each other; which part of the errors are explained by segmentation of bone, segmentation of prosthesis, segmentation of align, registration method, spatial resolution of image and/or other factors? This could be determined by performing a sensitivity analysis to determine the largest contributing factor for errors in migration measurement.



Table 10: Migration results for six different masks and corresponding mask of tibia bones: mean (+/- SD). Results greater than 0.1 mm or deg are highlighted. Abbreviations: Exp = experiment, RG = Region Grow, OC = Morphological Opening and Closing, px = pixel, PTM = prosthesis mask, ST = Small Threshold, 26c = 26 connectivity (parameter for region grow).

Exp	Mask prosthesis	Mask prosthesis (migrating)	Tx (mm)	Ty (mm)	Tz (mm)	Rx (deg)	Ry (deg)	Rz (deg)
2.0		PTM_RG	0.01 (0.02)	-0.01 (0.02)	-0.03 (0.02)	-0.03 (0.04)	0.09 (0.4)	-0.03 (0.03)
2.1		Prothesis_ST_OC_2px	0.02 (0.01)	0 (0.01)	-0.02 (0.01)	-0.02 (0.04)	0.05 (0.04)	-0.04 (0.02)
2.2		Prothesis_ST_RG_6c	0.03 (0.01)	0.02 (0.03)	0.02 (0.04)	0 (0.04)	0.03 (0.22)	-0.06 (0.03)
2.3		Prothesis_ST_RG_26c	0.02 (0)	0.02 (0.01)	0 (0.02)	0.01 (0.02)	0.16 (0.08)	-0.04 (0.01)
2.4		Prothesis_ST_OC_1px	0.02 (0)	0.01 (0.01)	0 (0.02)	0 (0.02)	0.06 (0.26)	-0.05 (0.02)
2.5		Prothesis_ST_RG_6c_Edit	0.06 (0.1)	0 (0.02)	-0.01 (0.09)	0.01 (0.04)	-0.67 (1.4)	-0.06 (0.04)

## DATASET B: MICROMANIPULATOR

**Set-up:** A cadaveric bone with a tibial component of size 5. The prosthesis was not fixed to the bone. Attached to the prosthesis is a micromanipulator for mechanical translation and rotation. The accuracy of the micromanipulator is 0.012 mm / 0.01 deg. Patient motion is simulated with phantom movement in between CT scans.

**Micromanipulator settings:** Rotation of 0.5, 1.0, and 1.5 degrees in z-axis of micromanipulator, which corresponds to the Y-axis in the CTRSA-software.

**CT data:** A standardized knee-prosthesis scan protocol was used. Data acquisition and processing were the same for the 24 CT volumes, **see table 11**.

Table 11: Overview of CT parameters of CT images used in dataset B.

Parameter	Setting
Scanner	Toshiba, Aquilion ONE
Slice Thickness (mm)	0.5
Pixel Spacing (mm\mm)	0.301\0.301
Number of Frames	640
Rows	512
Columns	512
Convolution Kernel	FC30
CT tube voltage (kVp)	120
Xray Tube Current (mA)	30
Scan Options	VOLUME_CT
Data collection Diameter	500
Focal spot	0.9\0.8

### Experiment 3: How many pixel dilation is needed?

During the course of the research, the question was posed, if the accuracy of CTBMA is affected by the segmentation masks. In this dataset, the segmentation is relatively straightforward with respect to experiment 1 and 2. This is due to the air between prosthesis and bone, making the segmentation limited to threshold and region grow. The masks were dilated and eroded to test if this affects the accuracy of CTBMA.

**Aim:** Determine amount of pixel dilation for the segmentation algorithm.

**Hypothesis:** The migration is more accurate when edges are included in segmentation (thus pixel dilation is better than normal / erode).

**Method:** Calculate migration for six different masks for the applied rotations.

- Data:
  - o Baseline image: zero rotation (002).
  - o Follow-up image: Positive rotation of 0 / 0.5 / 1.0 / 1.5 degrees around the Z-axis of micromanipulator, which corresponds to the Y-axis in the CTRSA-software.
- Segmentation:
  - o Prosthesis:

Number	Segmentation algorithm
1	Threshold + RG
2	Threshold + RG + 1 px dilation
3	Threshold + RG + 2 px dilation
4	Threshold + RG + 10 px dilation
5	Threshold + RG + 2 px erodation
6	Threshold + RG + 10 px erodation

- o Bone: threshold + region grow (select tibia bone) + Boolean operation (substraction: bone mask minus prosthesis mask).

- Registration:

- CTRSA-software version (07-12-2021).

### Results:

The migration results are represented in **figure 19 and 20**.

- Migration is negative for Y-axis (instead of positive in z-axis: the CT coordinate system versus micromanipulator coordinate system).
- The translation in X direction seems to be correlated with increasing rotation around the Y-axis.
- In all masks expect for 10 pixel erodation, a translation in Z-axis is seen during a specific follow-up moment.
- Total time for experiment:
  - Preparing data:  $\pm 2$  hours
  - Computational time:  $\pm 2$  hours (computer properties: Intel(R) Xeon(R) CPU quadcore, installed RAM 12.0 GB, NVIDIA Quadro FX 1700)
- The origin of the migrating coordinate system does not co-align with the center of rotation from the micromanipulator, **see figure 21**.

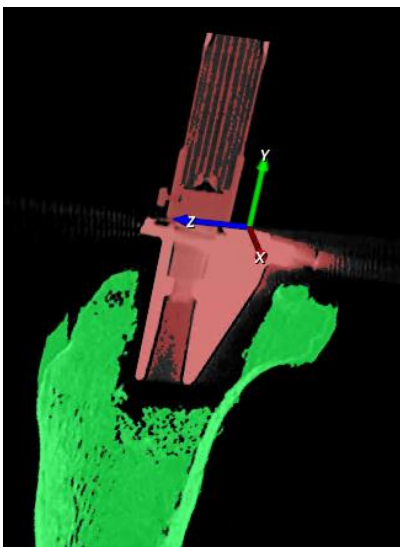


Figure 21: CT image with segmented tibia bone and tibia component with attached micromanipulator. Origin of coordinate system. This origin is determined by the center of a bounding box.

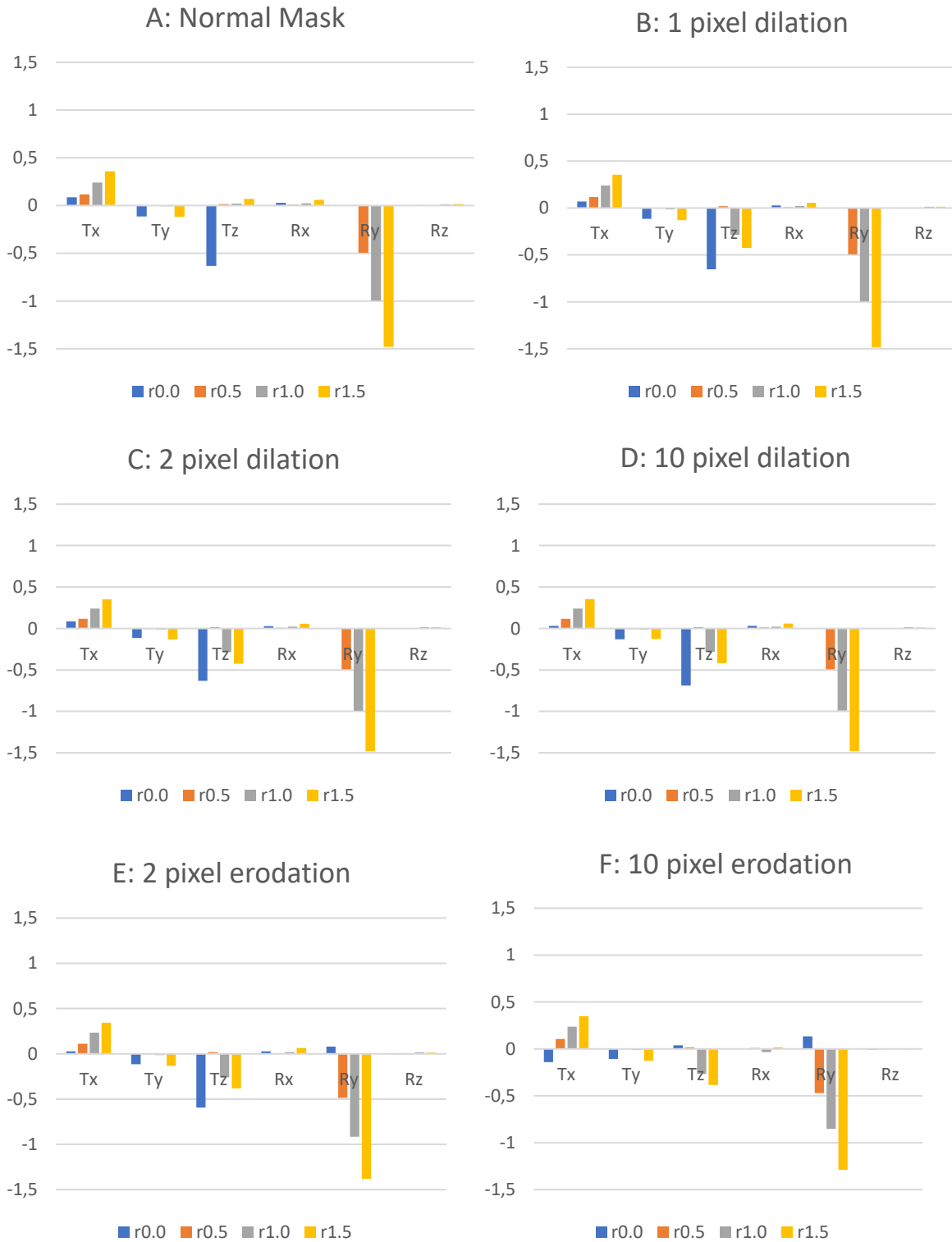


Figure 19: Migration results of experiment 3 with applied rotation around Z-axis for normal mask (A), 1 pixel dilation (B), 2 pixel dilation (C), 10 pixel dilation (D), 2 pixel erodation (E), and 10 pixel erodation (F). Migration results are given for four applied rotations around the Z-axis: 0 degrees (r0.0), 0.5 degrees (r0.5), 1.0 degrees (r1.0), and 1.5 degrees (r1.5).

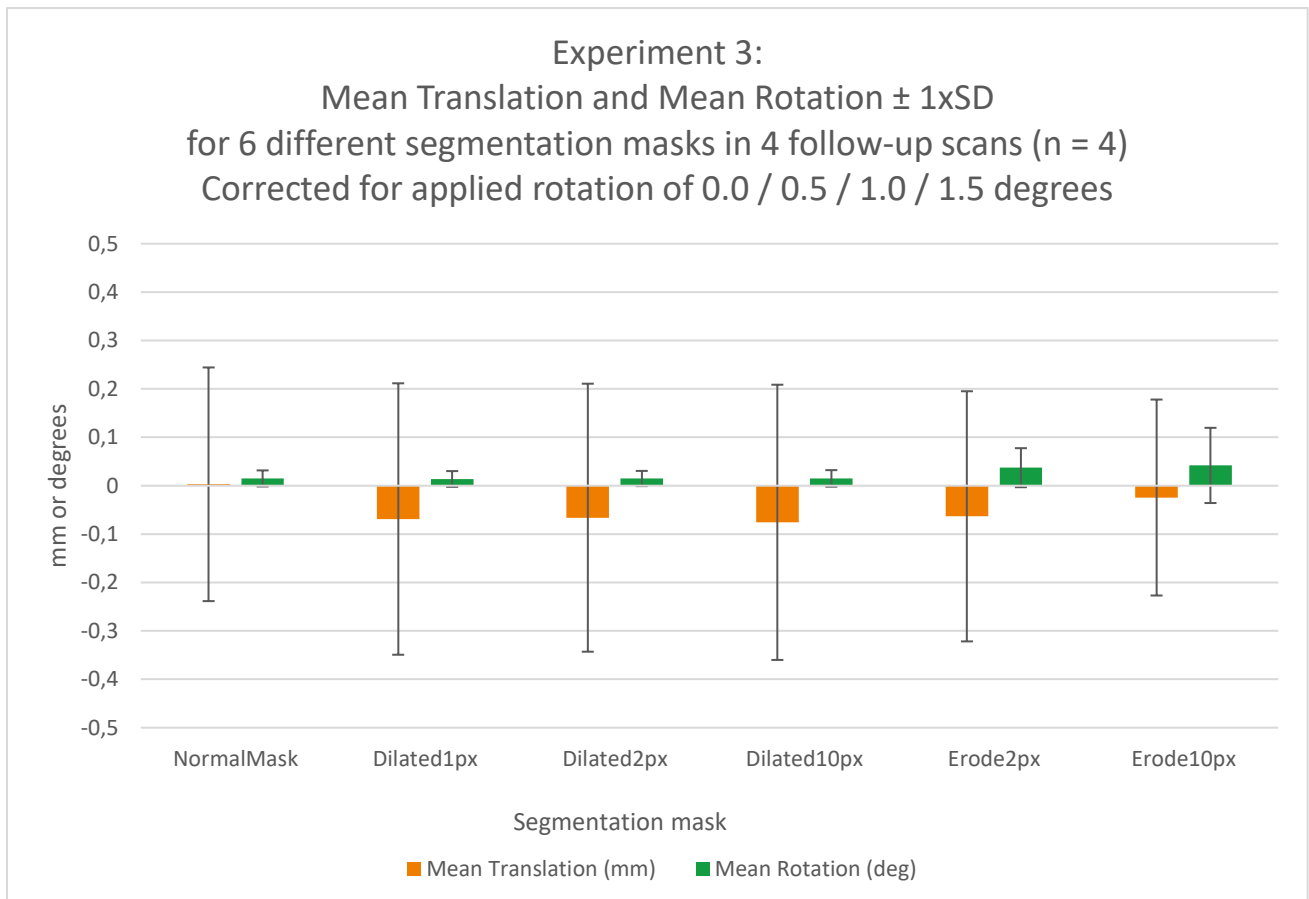


Figure 20: Migration results (mean  $\pm 1xSD$ ) of mean translation (blue bar) and mean rotation (grey bar) and the standard deviation (black vertical line with cap) for six different segmentation masks in four different follow-up scans (n = 4). Note that rotations are most relevant in this figure, as the input of the micromanipulator is set to specific rotations.

### Conclusion:

- Based on this experiment it seems that the normal mask is sufficient for measuring the applied rotation. Also, dilation of mask to include the edges seems not to be needed. An erosion of prosthesis mask could even result in less accurate measurement of applied rotation.
- The point of rotation does not co-align with the origin of coordinate system. A rotation around a point other than the origin results in a translation as well.
- In this version of CTRSA-software, the center of mass is determined by the center of a bounding box. In model-based RSA the center of mass is determined differently, this option could be valuable to be added to the CTRSA-software for comparing to model-based RSA.
- Applied rotation on micromanipulator is in the positive direction, measured rotation in CTRSA-software is in the negative direction.

### Discussion:

- This experiment contains one type of prosthesis, one type of CT scan, and only 4 follow-up images, therefore the results should be interpreted with care.
- One type of rotation (only rotation around Z-axis), therefore the accuracy of translation measurements is unknown.
- Prosthesis does not touch the bone, which results in air between the prosthesis and bone. Therefore, the segmentation is not representative to the clinical situation where the prosthesis touches the bone, as is seen in dataset A and C. Also, dilating the mask in this situation will only result in adding air to the masks. It is unknown how dilating the mask in a clinical situation would influence the migration results, since the prosthesis mask could include voxels belonging to other volumes than the prosthesis.
- The center of mass is determined by the whole mass of the micromanipulator, not just the tibia component of prosthesis. In future analysis, the segmentation mask of prosthesis should only include the tibia component and not the micromanipulator.

#### Experiment 4: Order of registration

**Aim:** Determine order of registration.

**Hypothesis:** Using prosthesis registration as starting point for bone registration results in less calculation time and in migration values closer to zero (considering no migration is expected).

**Method:**

- Data:
  - Baseline image: zero rotation (002).
  - Follow-up image: Rotation of 1.0 degrees around Z-axis of micromanipulator, which corresponds to the Y-axis in the CTRSA-software (see experiment 3).
- Segmentation:
  - Baseline image: Threshold + region grow 6c + normal mask (no dilation or erode) (see experiment 3).
- Registration:
  - Version CTRSA-software, date of use: 07/12/2021.
  - Three different analysis, which differ in the order of registration:
    1. Align > bone (align) > prosthesis (align).
    2. Align > bone (align) > prosthesis (bone).
    3. Align > prosthesis (align) > bone (prosthesis).Where, align refers to the initial alignment of the CT images.  
> refers to the order of registration.  
(align) / (bone) / (prosthesis) refers to the registration used as starting point for following registration.

**Results:**

The results of time and migration are given in **table 12**.

- Registration of reference based on align followed by migration based on align results in exactly the same migration results as registration of migration based on align followed by reference based on align. Thus: align > reference (align) > migrating (align) = align > migrating (align) > reference (align) in this dataset.
- The time it takes for the software for one single registration (thus for registration of two images) is between 1m41s and 1m48s. The total computational time of the three registrations together is therefore about 5 minutes in this dataset (computer properties: Intel(R) Xeon(R) CPU quadcore, installed RAM 12.0 GB, NVIDIA Quadro FX 1700).
- Migration results are equal for all three analysis.

Table 12: Total time elapsed for the three registrations (align, reference and migrating) for the three different orders of registration in one patient (n = 1). File name: Micromanipulator\_Rzp-002\_NoAR-r1.0-NormalMask1.0\_migration. Abbreviations: m = minute, s = seconds

Order of test	Order of registration	Time			Migration results					
		Align	Reference	Migrating	Tx	Ty	Tz	Rx	Ry	Rz
1	align > reference (align) > migrating (align)	1m41s	1.48s	1.45s	0.24	-0.01	0.02	0.02	-0.99	0.01
2	align > reference (align) > migrating (based on reference)	1m41s	1.46s	1.46s	0.24	-0.01	0.02	0.02	-0.99	0.01
3	align > migrating (align) > reference (based on migrating)	1m41s	1.44s	1.48s	0.24	-0.01	0.02	0.02	-0.99	0.01

**Conclusion and discussion:**

- The three different registration analysis result in same results for translation and rotation. The order is therefore interchangeable for this data.
- The difference in computational time for the three different order of registration is negligible.
- Experiment should be repeated in clinical data, since the registration could be more complex in *in vivo* compared to *in vitro*. This will be shown in experiment 6.

## DATASET C: CLINICAL DATA

In a randomized controlled trial, two types of TKA's were compared [24]. Data from this study included 18 pairs of CT images.

**CT data:** See **chapter 4 table 2** for the CT data of each patient.

The segmentation method, based on previous experiments, in the clinical setting is described in **figure 22**. The registration mentioned in this figure will be explained in experiment 5 and 6. Calculation of migration is explained in **chapter 3**.

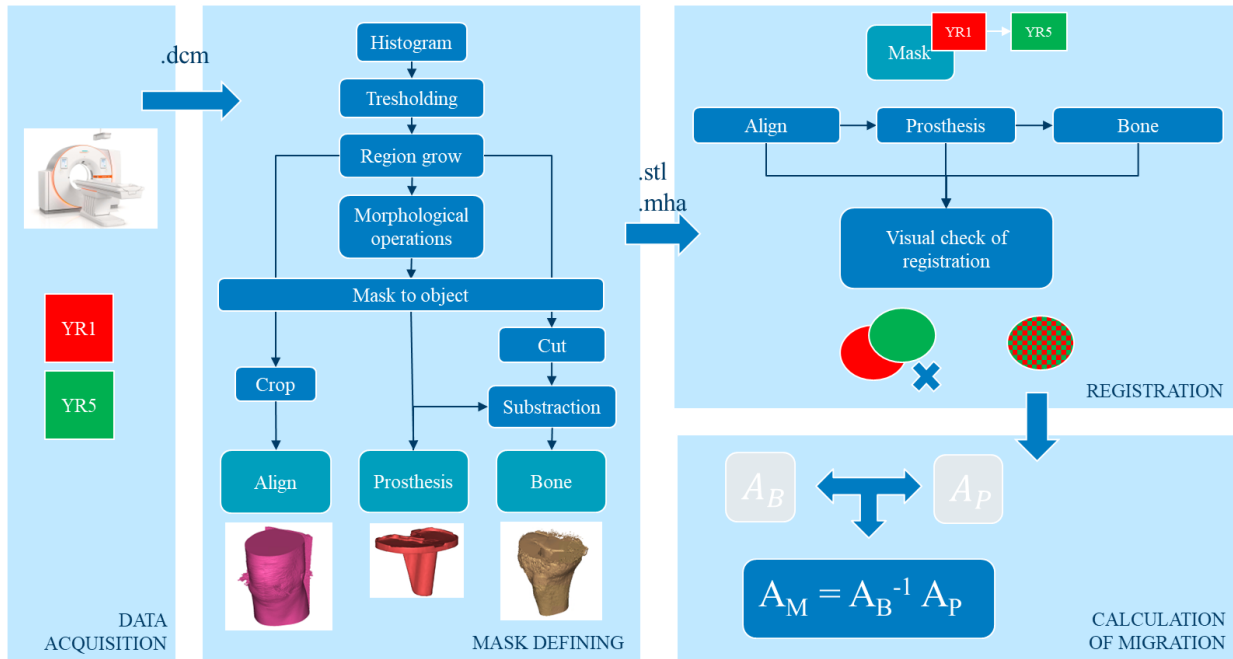


Figure 22: Schematic overview of CT-based migration analysis. Abbreviations: YR = year, dcm = dicom, stl = standard triangle language, mha = MetalImage Medical Format,  $A_M$  = Migration transform matrix,  $A_B$  = transform matrix of bone and  $A_P$  = transform matrix of prosthesis.

### Experiment 5: Which align mask to use?

**Aim:** Determine the align mask.

**Hypothesis:** Initial alignment of CT images is similar for different align masks.

**Method:** Try out segmentation + registration in five patients. Two of them had Persona prosthesis (PNS19 + PNS22) and two had NexGen (PNS21 + PNS25). One patient (PNS15) was chosen to check the method when follow-up image contained two knees in the CT image.

- Data:
  - Baseline image: CT YR1.
  - Follow-up image: CT YR5.
- Segmentation:
  - Baseline image: segmentation algorithm for prosthesis and bone see figure 22.

Three different masks for align (align refers to the initial alignment of CT images):

1. Align with total knee (soft tissue included).
  - a. Segmentation algorithm: threshold to include entire knee (soft tissue, bone and prosthesis).
2. Align with prosthesis (femoral + tibial component) .
  - a. Segmentation algorithm: threshold to include prosthesis.
3. Align with tibial component (use same mask as prosthesis mask)
  - a. Segmentation algorithm: threshold + region grow + morphological operations.

- Registration:
  - Version CTRSA-software, date of use: 07/12/2021.
  - The order of registration is the same for all patients: align > reference (align) > migrating (align).

The align mask is chosen based on the following arguments: visually checked if the registration was successful in all five patients, time of registration (less is better), low migration values (this is expected if registration is performed well) and time of segmentation (less is better).

### Results:

The results for the three different masks for align:

1. Successful registration in all five patients. Also when follow-up image contains two knees in CT image. The segmentation time was less than 1 minute, unless the leg touched the other leg. Then additional time was needed to separate these using split mask or crop function (both functions in Mimics).
2. Incorrect registration in PNS19 and PNS15. Align mask contained many additional pixels which were not the prosthesis. It was very time consuming to manually remove these pixels.
3. No visual registration to check, therefore, results are only reported for PNS19. No extra segmentation time was needed, since the same mask is used as is needed for prosthesis-prosthesis registration.

The migration values of PNS19 for the three different align mask are seen in **table 13**. The total translation and total rotation of five patients are visualized in **figure 23**.

Table 13: Migration results for experiment 7: which align mask to use? The migration of PNS19 is given for three different align masks used. Abbreviations: Exp = experiment.

Corresponding exp name in files	Mask for align	Tx	Ty	Tz	Rx	Ry	Rz
Exp5b	Total knee	0.05	-0.21	0.03	-0.08	0.07	0.15
Exp5	Prosthesis tibia + femur	17.10	-52.53	5.90	7.62	1.71	-11.70
Exp5a	prosthesis tibia	-0.01	-0.20	0.03	-0.08	0.07	0.15

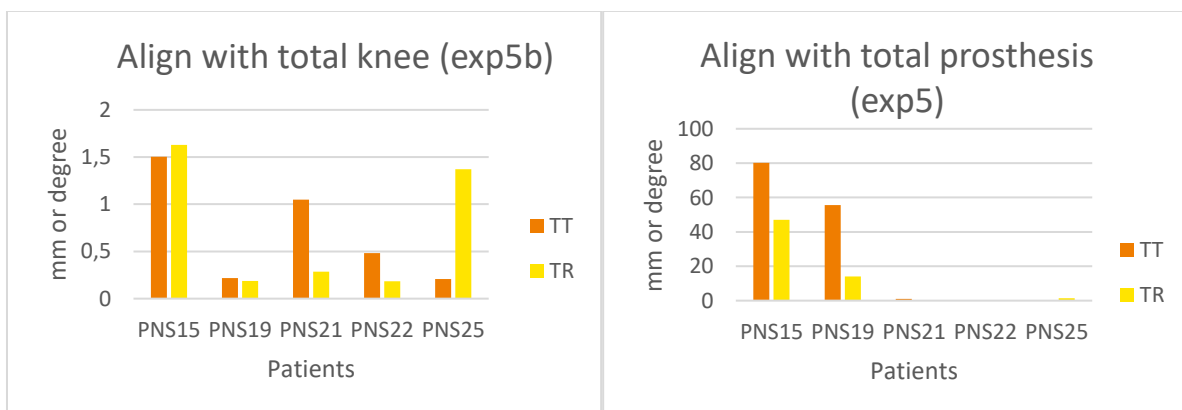


Figure 23: Total Translation (mm) and Total Rotation (degrees) of 5 patients for two different align masks: knee and total prosthesis. Be aware of the differences in the Y-axis.

### Conclusion and Discussion:

- The alignment with total knee was chosen to use in the entire dataset.
- Based on this experiment it is not ruled out that using the tibia component as align mask is inferior to the whole knee as align mask.



## Experiment 6: Order of registration

**Aim:** Determine order of registration.

**Hypothesis:** The registration of prosthesis is better than on bone, therefore, registration of bone with prosthesis as starting point results in more accurate registrations.

**Method:** Repeat of experiment 4 (order of registration) in clinical data. However unknown, the migration is expected to be around zero. Migration values other than zero, were expected to be less accurate registrations.

- Data:
  - Baseline image: CT YR1
  - Follow-up image: CT YR5
- Segmentation:
  - Baseline image: see segmentation algorithm in **figure 22**.
- Registration:
  - Version CTRSA-software, date of use: 07/12/2021
  - Three different analysis, which differ in the order of registration:
    1. Align > bone (align) > prosthesis (align).
    2. Align > bone (align) > prosthesis (bone).
    3. Align > prosthesis (align) > bone (prosthesis).Where, align refers to the initial alignment of the CT images.  
> refers to the order of registration.  
(align) / (bone) / (prosthesis) refers to the registration used as starting point for following registration.

The order of registration is compared between all patients with visual good registration ( $n = 16$ ) and a subset of patients ( $n = 12$ ) where the patients with one of the two CT images contained two knees, negatively affecting the spatial resolution.

**Results:** The three-dimensional plots of translation and rotation measurements of the patients are seen in **table 14**. The ellipsoid is fitted around all data, making it useful for intuitive and comparative interpretations, as well as for visual outlier detection. For translations, the ellipsoid of analysis 2 and 3 are smaller than for analysis 1. For rotations the ellipsoid of analysis 1 and 2 are similar, in contrast to that of analysis 3, which shows a smaller volume. All ellipsoids are smaller in the subset of patients ( $n = 12$ ) compared to all patients ( $n = 16$ ).

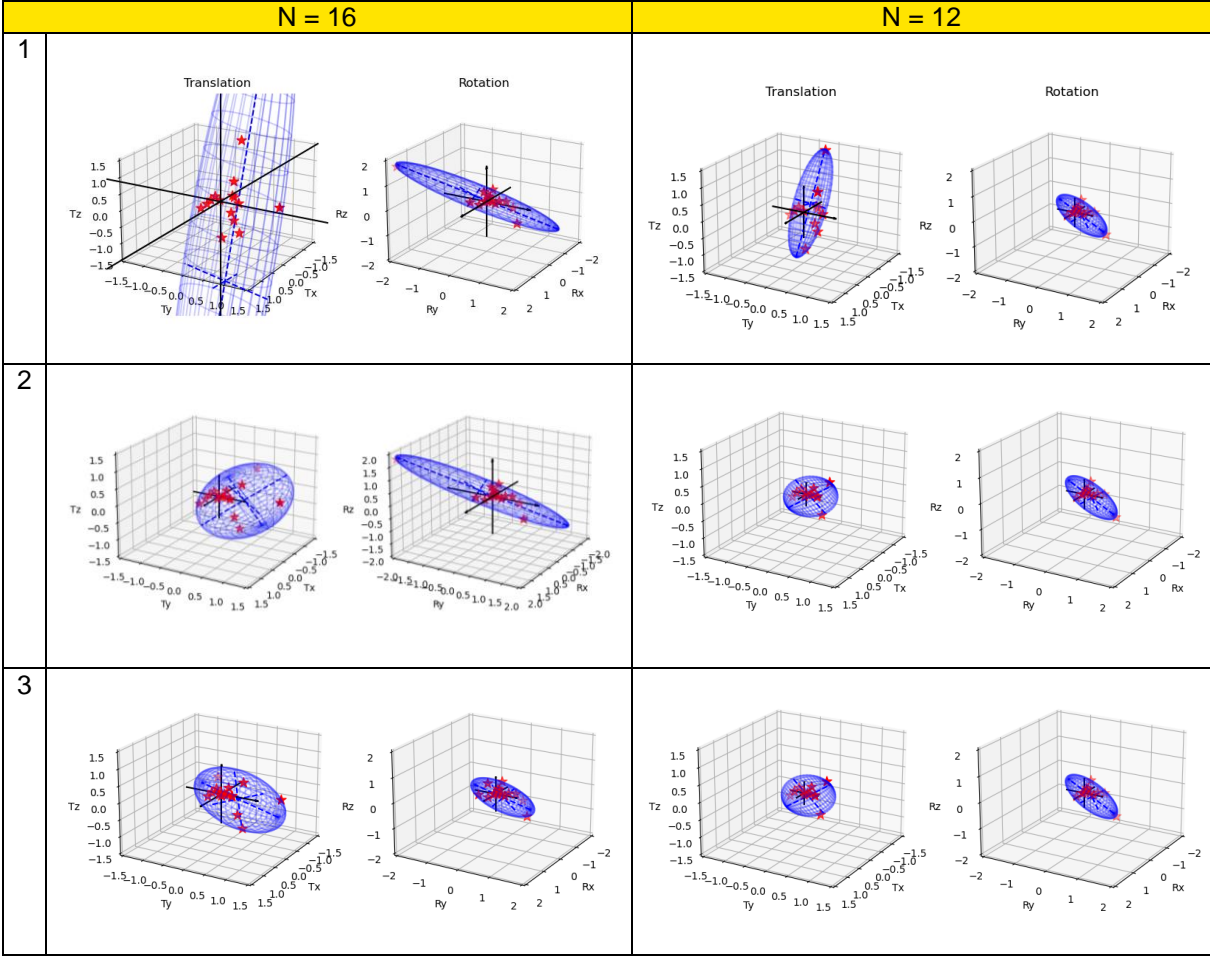
### Conclusion:

For this version of the CTRSA-software, the outliers can be explained by the pixel size of the CT images. We choose number 3 for the order of registration, because this analysis shows the smallest ellipsoid for all patients, which would be the most accurate registration considering the results are expected to be close to zero.

### Discussion:

The results are given with an older version of CTRSA-software, it is therefore unknown if the choice for order of registration order would be the same in the newer version of CTRSA-software. This is because some critical transformation function may have been changed in the newer version of CTRSA-software. See section below regarding the differences between older and newer version of CTRSA-software.

Table 14: Three-dimensional scatterplot of total translation and total rotations of 16 patients (left column) and 12 patients (right column) with fitted ellipsoid (blue ellipsoid) around the data of patients (red stars). The intersection of the blue dotted lines inside the ellipsoid represent the middle of the ellipsoid. The origin of the axes (black arrows) is positioned at (0, 0, 0) and length of these axes correspond to the size of the ellipsoid. Three different analyses are shown for both number of patients which corresponds with the following order of registration: (1) Align > bone (align) > prosthesis (align). (2) Align > bone (align) > prosthesis (bone). (3) Align > prosthesis (align) > bone (prosthesis).



### Newer version of CTRSA-software

All experiments were conducted with an older version of software, in contrast to the results reported in chapter 3 which were conducted with a newer version of the software. Old version refers to the versions before 02-04-2022 and new version refers to version after 02-04-2022 till 18-06-2022.

The functional differences between the older version and newer version of CTRSA-software (software for CTBMA):

- Method for determining the center of mask:
  - Old version: the middle of a bounding box.
  - New version: calculation of center of mask.
- Changes in coordinate transformation, see **chapter 3**:
  - Older version:  $A_M = A_P^{-1} \cdot A_B$
  - Newer version:  $A_M = A_B^{-1} \cdot A_P$

Compare results new vs old version:

- Dataset A: zero migration experiment 2.4:

CTRSA version (date of use)	Analysis	Tx	Ty	Tz	Rx	Ry	Rz
Old version (02/12/2021)	Kadaver2509_LeftKnee-SEMAR_S01-SEMAR_S05-Experiment2.4	0.02	0.02	0.02	0.03	-0.28	-0.04
Old version (02/12/2021)	Kadaver2509_LeftKnee-SEMAR_S01-S02_SEMAR-FU2	0.01	-0.00	-0.02	-0.01	0.27	-0.05
Old version (02/12/2021)	Kadaver2509_LeftKnee-SEMAR_S01-S03_SEMAR-FU3	0.02	0.02	0.01	0.01	0.26	-0.08
Old version (02/12/2021)	Kadaver2509_LeftKnee-SEMAR_S01-S04_SEMAR-FU4	0.01	0.01	-0.00	-0.02	0.01	-0.03

CTRSA version (date of use)	Analysis	Tx	Ty	Tz	Rx	Ry	Rz
New version (07/06/2022)	Kadaver2509_LeftKnee-SEMAR_S01-SEMAR_S05-Experiment2.4	0.02	0.02	0.02	0.04	-0.19	-0.04
New version (07/06/2022)	Kadaver2509_LeftKnee-SEMAR_S01-S02_SEMAR-FU2	0.02	-0.00	-0.02	-0.01	-0.02	-0.04
New version (07/06/2022)	Kadaver2509_LeftKnee-SEMAR_S01-S03_SEMAR-FU3	0.03	0.00	-0.02	0.00	0.02	-0.06
New version (07/06/2022)	Kadaver2509_LeftKnee-SEMAR_S01-S04_SEMAR-FU4	0.02	0.01	-0.00	-0.02	0.02	-0.03

- Dataset B: Micromanipulator with rotation of 1.5 degrees:

CTRSA version (date of use)	Analysis	Tx	Ty	Tz	Rx	Ry	Rz
New version (07/06/2022)	Micromanipulator_Rzp-002_NoAR-r1.5-NormalMask1.5	0.24	-0.12	0.05	0.06	-1.48	0.01
Old version (07/12/2021)	Micromanipulator_Rzp-002_NoAR-r1.5-NormalMask1.5	0.36	-0.11	0.07	0.06	-1.48	0.01

### Conclusions:

- Results in zero-migration measurement are comparable.
- Results in data with micromanipulator are similar for rotations, for the translation the results differ slightly with a maximum value of 0.12 mm for Tx in this specific data.

## APPENDIX B: BLAND-ALTMAN PLOTS

The Bland-Altman plots of the translations and rotations.

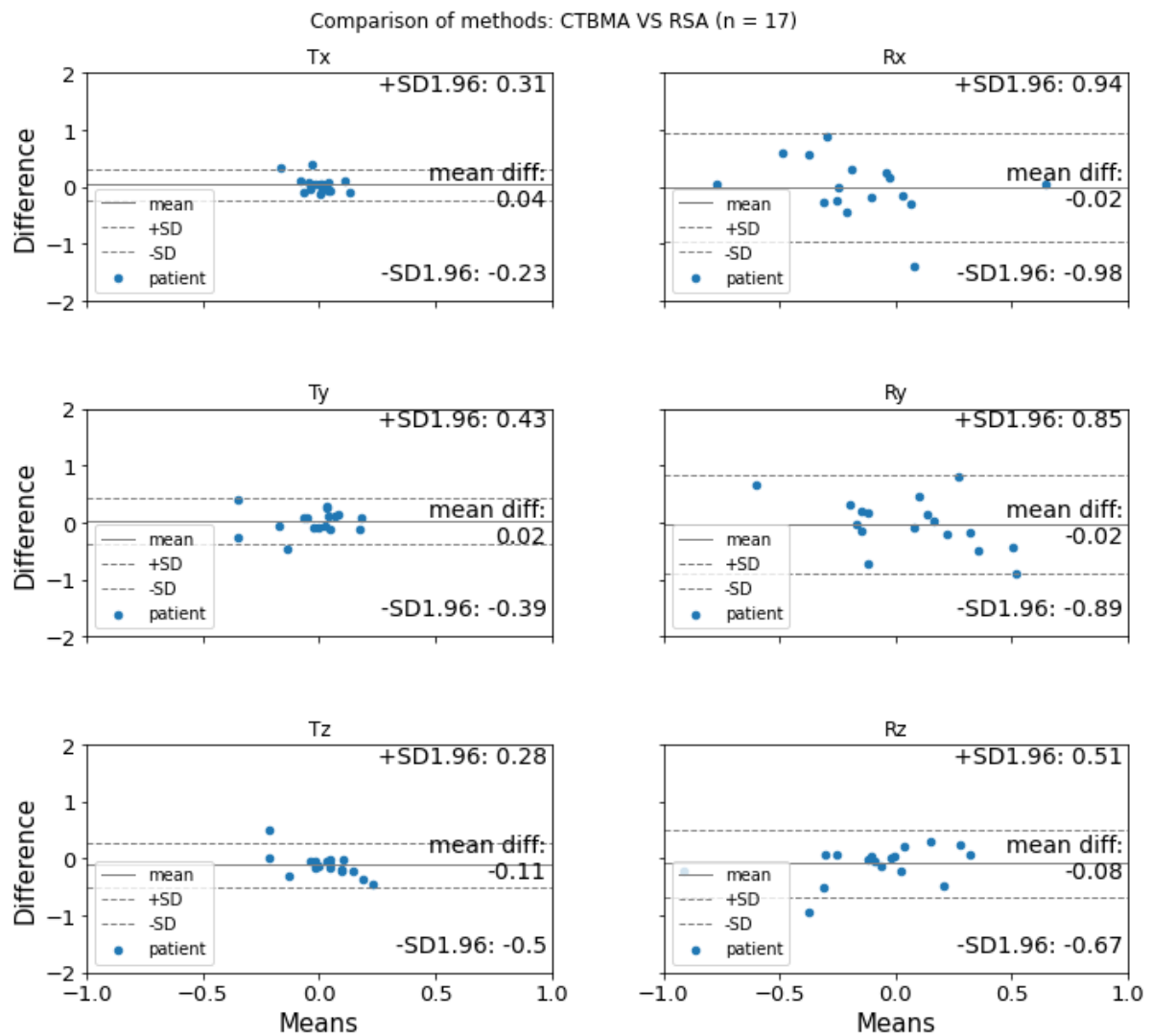


Figure 24: Bland-Altman plots of translations (mm) in X, Y, and Z-axes (left panel) and rotations (degrees) around the X, Y, and Z-axes (right panel) of 17 patients (blue dots) for comparison between the two methods: CTBMA and RSA. The solid line is the mean difference between the two methods. The dashed lines represent the limits of agreement. Differences = CTBMA-RSA, Means = (CTBMA+RSA)/2, SD = Standard Deviation, mean diff = mean difference between the two methods.

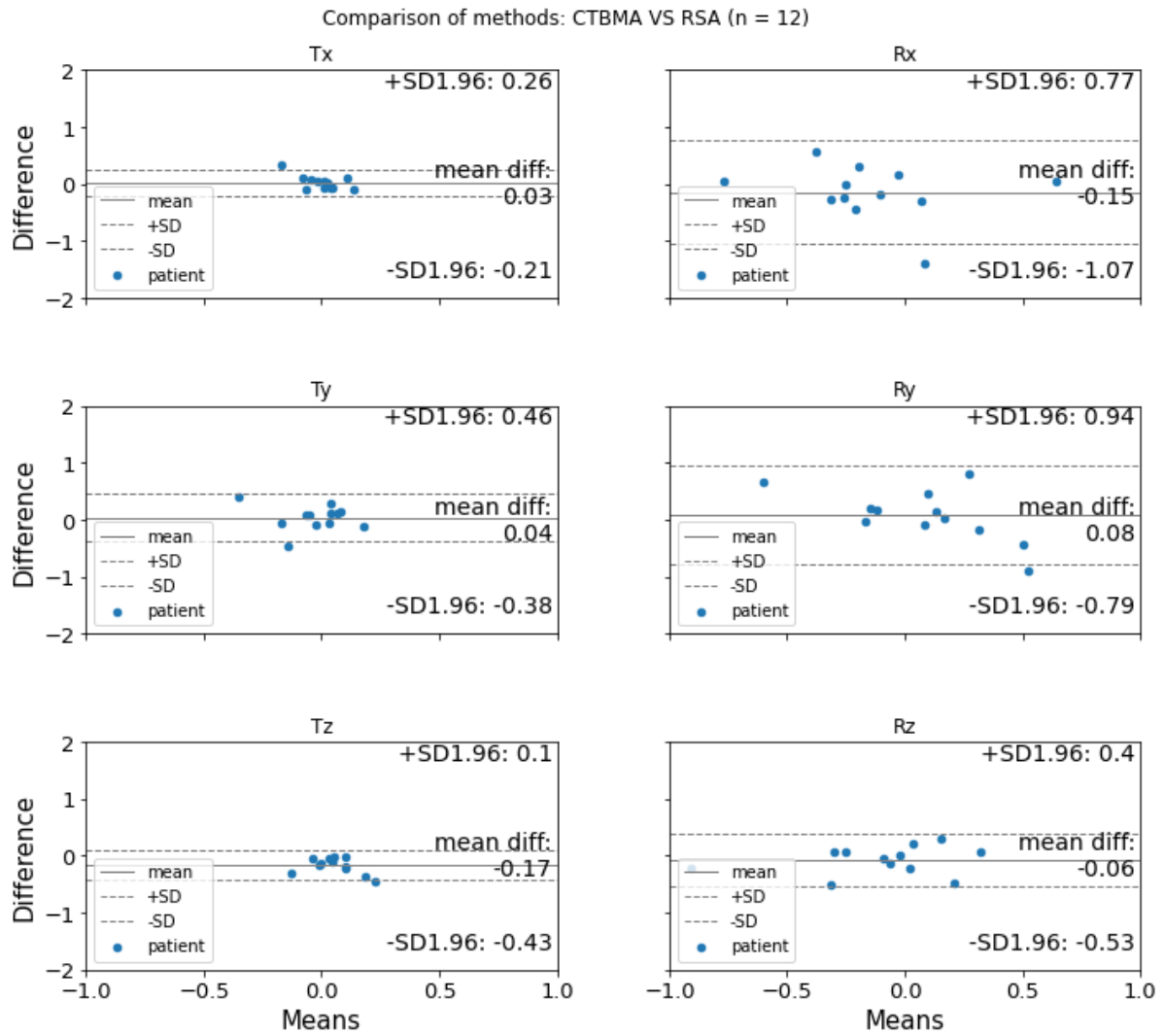


Figure 25: Subanalysis of CT images of all patients with only one knee in the baseline and follow-up CT image. Bland-Altman plots of translations (mm) in X, Y, and Z-axes (left panel) and rotations (degrees) around the X, Y, and Z-axes (right panel) of 12 patients (blue dots) for comparison between the two methods: CTBMA and RSA. The solid line is the mean difference between the two methods. The dashed lines represent the limits of agreement. Differences = CTBMA-RSA, Means = (CTBMA+RSA)/2, SD = Standard Deviation, mean diff = mean difference between the two methods.

# APPENDIX C: HISTOGRAM PLOTS



Figure 26: Histogram plots of translations (mm), rotations (mm), TT (mm) and TR (degrees) of A) CTBMA, B) RSA and C) differences (CTBMA – RSA). The frequency represent the number of patients and x, y, and z represents the corresponding axis.



